UNIVERSIDAD DE CONCEPCIÓN

Centro de Investigación en
Ingeniería Matemática (CI^{2}MA)

Theoretical analysis and numerical validation of an inverse problem in a SIS reaction–diffusion system, Part 1: Identification of transmission and recovery rates

Aníbal Coronel, Fernando Huancas,
Mauricio Sepúlveda

PREPRINT 2026-29

SERIE DE PRE-PUBLICACIONES

Theoretical analysis and numerical validation of an inverse problem in a SIS reaction–diffusion system, Part 1: Identification of transmission and recovery rates

Aníbal Coronel[a,*], Fernando Huancas[b], Mauricio Sepúlveda[c]

[a]*Departamento de Ciencias Básicas–Centro de Ciencias Exactas, Facultad de Ciencias, Universidad del Bío-Bío, Campus Fernando May, Chillán 378000, Chile*
[b]*Departamento de Matemática, Facultad de Ciencias Naturales, Matemáticas y del Medio Ambiente, Universidad Tecnológica Metropolitana, Las Palmeras No. 3360, Ñuñoa–Santiago 7800003, Chile*
[c]*Centro de Investigación en Ingeniería Matemática (CI²MA) y Departamento de Ingeniería Matemática (DIM), Universidad de Concepción, Casilla 160-C, Concepción, Chile*

Abstract

This work is the first article in a series of studies on inverse problems for this class of epidemiological models. It establishes mathematical and computational foundations by focusing on reaction coefficients, while subsequent parts address the incidence and other unknown model components. The mathematical model is a generalized susceptible-infected-susceptible (SIS) epidemic model with spatial population displacement. We formulate the determination of transmission and recovery rates from final-time observations as a constrained optimization problem. We study existence and uniqueness for the state system, existence of a minimizer, the adjoint problem, first-order necessary optimality conditions, continuous dependence of the state and adjoint solutions, and conditional uniqueness on a fixed-mean admissible subset. We also present numerical experiments for a finite-dimensional parameter-identification problem.

Keywords: Inverse problem, SIS, reaction–diffusion systems.

*Corresponding author
Email addresses: acoronel@ubiobio.cl (Aníbal Coronel), fhuancas@utem.cl (Fernando Huancas), mauricio@ing-mat.udec.cl (Mauricio Sepúlveda)

1. Introduction

The current literature thoroughly documents the mathematical modeling of epidemic spread [1–7]. Despite the advances, there are still aspects where mathematical analysis needs to be precise; an example of such a case is the problem of identification of the reaction and diffusion terms from observations of state variables. In a broad sense, the approaches used to model the dynamics of epidemics are based on differential and difference equations, both deterministic and stochastic. One of the most used methodologies to formulate those mathematical models is the compartmental approach, pioneered by Kermack-McKendrick [8]. In this context, the most basic model considers that the total population N is divided into two classes of individuals called susceptible and infected, denoted by S and I. Then, assuming that the compartment populations change by direct contact of infected individuals with susceptible ones or after having completed the infection period, the following mathematical model is deduced

$$\frac{dS}{dt} = -\beta SI + \gamma I, \quad \frac{dI}{dt} = \beta SI - \gamma I. \tag{1}$$

Here, βSI models the interaction of infected and susceptible individuals by applying the mass-action law, and γI models the recovery.

The model (1) is generalized into a reaction–diffusion system by assuming that spatial dispersion significantly impacts the disease dynamics and obtain the model

$$\frac{\partial S}{\partial t} - d_S \Delta S = -\beta SI + \gamma I, \quad \frac{\partial I}{\partial t} - d_I \Delta I = \beta SI - \gamma I. \tag{2}$$

The strictly positive constants d_S and d_I are the diffusion coefficients, which account for the spatial mobility of the population. It is worth noting that model (2) can be further generalized to include other aspects affecting the dynamics of spread. Particularly, we distinguish four possible groups of generalized models. Specifically, we extend the model to account for: the spatio-temporal dependence of the reaction coefficients β and γ; the generalization of the mass-action incidence through non-linear incidence functions [9–12]; the inclusion of a non-linear recovery term [13]; and the incorporation of a generalized diffusion matrix [14–17]. In the present work, we focus on the analytical and numerical investigation of the inverse problem of identifying spatio-temporal reaction coefficients, assuming an observed profile of the infected population at a fixed time.

More precisely, in this paper, we consider that the spatio–temporal dynamics of the disease are governed by the following reaction–diffusion SIS model:

$$
\begin{aligned}
S_t - d_S \Delta S &= -\beta(x,t) f(S,I) + \gamma(x,t) I, && \text{in } Q_T := \Omega \times (0,T], && (3)\\
I_t - d_I \Delta I &= \beta(x,t) f(S,I) - \gamma(x,t) I, && \text{in } Q_T, && (4)\\
\nabla S \cdot \boldsymbol{\eta} &= \nabla I \cdot \boldsymbol{\eta} = 0, && \text{on } \Gamma := \partial\Omega \times (0,T], && (5)\\
(S,I)(x,0) &= (S_0, I_0)(x), && \text{in } \Omega, && (6)
\end{aligned}
$$

where $\Omega \subset \mathbb{R}^d$ $(d \geq 1)$ is a bounded open set with a smooth boundary $\partial\Omega$, and $\boldsymbol{\eta}$ denotes the outward unit normal vector to $\partial\Omega$, $Q_T := \Omega \times (0,T]$ denotes the spatio-temporal domain and $\Gamma := \partial\Omega \times (0,T]$ represents the boundary; $S(x,t)$ and $I(x,t)$ correspond to the densities of susceptible and infected individuals, respectively; $S_0(x)$ and $I_0(x)$ are initial distributions; the transmission and recovery processes are characterized by the spatio-temporally dependent coefficients $\beta(x,t)$ and $\gamma(x,t)$, respectively; the function $f(S,I)$ introduces a generalized nonlinear incidence rate. The boundary conditions (5) imply a null flux across $\partial\Omega$, suggesting that the population remains isolated within the geographic domain Ω.

In this paper, we investigate the inverse problem of identifying the spatio-temporal coefficients (β, γ) in the reaction–diffusion system (3)–(6), based on available observational data for the susceptible and infected populations; more precisely, we address the inverse problem:

$$
\left.
\begin{array}{l}
\text{Given } T, d_S, d_I \in \mathbb{R}^+, \text{ the functions } S_0, I_0, S^{obs}, \text{ and } I^{obs} \text{ defined} \\
\text{on } \Omega, \text{ and the function } f, \text{ find the functions } \beta \text{ and } \gamma \text{ defined} \\
\text{on } Q_T, \text{ such that } (S,I)(\cdot,T), \text{ the solution of (3)-(6) at } t=T, \\
\text{is as close as possible to the observation data } (S^{obs}, I^{obs}).
\end{array}
\right\} \qquad (7)
$$

We notice that the problem (7) is introduced to validate the proposed mathematical models with experimental data or to solve the well-known model calibration problems. We cast the parameter identification problem into an optimal control framework by defining an appropriate cost functional that measures the discrepancy between the predictions of the model (3)-(6) and the observational data.

To formalize the optimal control problem used to analyze (7), we introduce the cost function and the admissible set as follows

$$
\begin{aligned}
J(S,I) = \frac{1}{2}\left\|(S,I)(\cdot,T) - (S^{obs}, I^{obs})\right\|^2_{[L^2(\Omega)]^2} \\
+ \frac{\Lambda}{2}\iint_{Q_T}\left(|\nabla_x\beta|^2 + |\nabla_x\gamma|^2\right)\, dx\, dt,
\end{aligned} \tag{8}
$$

$$
\begin{aligned}
\mathcal{U}_{ad} = \Big\{ (\beta,\gamma) \in [C^{\alpha,\alpha/2}(\overline{Q}_T)]^2 \cap [L^2(0,T;H^1(\Omega))]^2 \ : \\
\|(\beta,\gamma)\|_{[C^{\alpha,\alpha/2}(\overline{Q}_T)]^2} + \|(\beta,\gamma)\|_{[L^2(0,T;H^1(\Omega))]^2} \leq M \quad \text{and} \\
(\beta,\gamma)(x,t) \in [\beta^{\perp},\beta^{\top}] \times [\gamma^{\perp},\gamma^{\top}] \subset \mathbb{R}^2_+ \text{ on } \overline{Q}_T \ \Big\},
\end{aligned} \tag{9}
$$

with $\Lambda \geq 0$. Here and throughout, ∇_x and Δ_x denote differentiation with respect to the spatial variable only. Thus, the regularization penalizes spatial, but not temporal, variations of the coefficients β and γ. The first term of J is introduced to make mathematical precise sense of the term "as close as" in (7), and the second term is proposed to regularize the cost function with an appropriate selection of the regularization parameter Λ. Then, the inverse problem (7) is reformulated as the constrained optimization problem

$$
\left.
\begin{aligned}
&(\overline{\beta},\overline{\gamma}) \in \underset{(\beta,\gamma)\in\mathcal{U}_{ad}}{\arg\min}\ \mathcal{J}(\beta,\gamma), \quad \mathcal{J}(\beta,\gamma) = J(S_{(\beta,\gamma)}, I_{(\beta,\gamma)}), \\
&\text{subject to } (S_{(\beta,\gamma)}, I_{(\beta,\gamma)}) \text{ solution of (3)-(6).}
\end{aligned}
\right\} \tag{10}
$$

We notice that $\mathcal{J}$ denotes the reduced cost functional with $(S_{(\beta,\gamma)}, I_{(\beta,\gamma)})$ the solution of (3)-(6) with coefficients (β,γ). The notation $L^2(\Omega)$ and $C^{\alpha,\alpha/2}(\overline{Q}_T)$ is used for the Lebesgue and Hölder spaces [19–22].

The main results of this paper focus on establishing the well-posedness of the optimal control problem and developing its numerical solution, providing simulations that complement and illustrate the analytical findings. To perform the rigorous mathematical analysis of the optimization problem (10), we consider the following assumptions:

(A1) The set $\Omega \subset \mathbb{R}^d$ is an open bounded and convex set with smooth boundary of class $C^{2+\alpha}$.

(A2) The initial condition is assumed to have the regularity requirements $(S_0, I_0) \in [C^{2+\alpha}(\overline{\Omega})]^2$ such that $(S_0,I_0)(x) \in [0,\infty)^2$ on Ω, and satisfying the compatibility conditions $\partial_\eta S_0 = \partial_\eta I_0 = 0$ on $\partial\Omega$.

(A3) The function $f : [0,\infty)^2 \to \mathbb{R}_+$ is a function satisfying the properties: $f \in C^{2+\alpha}_{loc}([0,\infty)^2)$; f is an increasing function of both variables on $[0,\infty)^2$; and $f(S,I) > 0$ for $S > 0$, $I > 0$, and $f(0,0) = f(0,I) = f(S,0) = 0$. Furthermore, when $d_S \neq d_I$, it is assumed that f satisfies at least one of the following global growth restrictions for all $S, I \geq 0$:

$$f(S,I) \leq c_1(S^q + I^q) + c_2,$$

for $q \in [1, 1 + 4/d)$ and some strictly positive constants c_1 and c_2.

(A4) The reaction coefficients are such that $(\beta,\gamma) \in \mathcal{U}_{ad}$ with $\mathcal{U}_{ad}$ defined in (9) and the diffusion coefficients d_S and d_I are positive.

(A5) The functions S^{obs} and I^{obs} belong to $C^{2+\alpha}(\overline{\Omega})$. and satisfying the compatibility conditions $\partial_\eta S^{obs} = \partial_\eta I^{obs} = 0$ on $\partial\Omega$.

In a broad sense, the assumptions (A1)-(A4) and (A5) are related with the well-posedness of the state equations and the adjoint system, respectively. The condition of positivity of the initial conditions, given in (A2) is required to get the positivity of the solution of the system (3)-(6). The assumptions on the incidence function f in (A3) (see [18]) reflect the biological requirement that the interaction be positive only when both populations coexist, and null otherwise.

From an analytical perspective, and within the framework of optimal control theory, we establish seven main results: (i) the existence and uniqueness of global classical solutions for (3)–(6); (ii) the existence of an optimal solution for the optimization problem (10); (iii) the formulation of the corresponding adjoint system; (iv) the derivation of a first-order necessary optimality condition for (10); (v) the stability of the direct problem solution with respect to the reaction coefficients; (vi) the stability of the adjoint problem solution with respect to the reaction coefficients and observational data; and (vii) a condition ensuring uniqueness on a fixed-mean admissible subset. In particular, if the optimal control is an interior point of the admissible set so that arbitrary signed variations are allowed, the optimal coefficients formally satisfy the following elliptic system:

$$\begin{aligned}
&-\Lambda\Delta_x\overline{\beta} = -f(\overline{S},\overline{I})(p_2 - p_1), && \text{in } Q_T,\\
&-\Lambda\Delta_x\overline{\gamma} = \overline{I}(p_2 - p_1), && \text{in } Q_T,\\
&\nabla_x\overline{\beta}\cdot\boldsymbol{\eta} = \nabla_x\overline{\gamma}\cdot\boldsymbol{\eta} = 0, && \text{on } \Gamma,
\end{aligned}$$

where (p_1, p_2) are the solutions of the adjoint system (see (39)–(42) below). This theoretical finding is also supported computationally; an equivalent discretization exhibits a consistent behavior regarding the discrete necessary optimality condition within the numerical scheme considered for the parameter identification problem.

In the numerical setting, we compute parametric sensitivities using a numerical-gradient approach [23]. We discretize the state system (3)–(6) using a finite difference scheme and solve the resulting finite-dimensional problem with a black-box constrained optimization procedure. Lastly, we present three numerical experiments illustrating the parameter-identification procedure.

We remark that there are several works focused on the analytical approaches for optimal control problems for reaction–diffusion problems, for instance [24–34]. Particularly, the study of the inverse problem (10) was initiated by Xiang and Liu in [34], where the authors develop a well-detailed analysis of one-dimensional ($d = 1$) with (β, γ) space dependent functions and $f(S, I) = SI/(S + I)$. An extension to $d \geq 1$ was developed in [27], by introducing appropriate assumptions and functional framework such that the results of [34] are still valid in higher spatial dimensions. Some advances, in order to research the application of the methodology to similar systems and to define the consistent general assumptions, are recently given in [26, 35], where the authors consider (β, γ) space dependent functions and $f(S, I) = S^q I^p$, for $p, q \in \mathbb{R}_+$.

The remainder of this paper is organized as follows. In Section 2, we present the mathematical analysis and results concerning the state system. Section 3 is devoted to the theoretical analysis of the optimal control framework and the corresponding inverse problem. Finally, Section 4 describes the numerical discretization scheme, details the optimization algorithm, and presents the numerical simulations that illustrate our findings.

2. Analysis and results of the state system.

2.1. Well-posedness of the state system.

Lemma 1. *Suppose that assumptions (A1)–(A4) are satisfied. Let (S, I) be the unique positive classical solution of the state system (3)–(6) defined on $\overline{Q}_T$. Then, there exists a uniform positive constant $C > 0$, depending only on Ω, T, d_S, d_I, $\mathcal{U}_{ad}$, and the initial data $\|(S_0, I_0)\|_{[L^\infty(\Omega)]^2}$, such that*

$$\|S(\cdot, t)\|_{L^\infty(\Omega)} + \|I(\cdot, t)\|_{L^\infty(\Omega)} \leq C, \quad \forall t \in [0, T]. \tag{11}$$

Proof. Firstly, summing the equations (3) and (4) and rearranging the initial and boundary conditions, we deduce the following initial-boundary value problem

$$
\begin{aligned}
(S+I)_t - d_S\Delta S - d_I\Delta I &= 0, && \text{in } Q_T, && (12)\\
\nabla(S+I)\cdot\boldsymbol{\eta} &= 0, && \text{on } \Gamma, && (13)\\
(S+I)(x,0) &= (S_0+I_0)(x), && \text{in } \Omega. && (14)
\end{aligned}
$$

Integrating (12) over Ω, the Neumann boundary conditions imply the conservation of the total population:

$$
\frac{d}{dt}\int_\Omega (S+I)\,dx = 0 \quad \text{then} \quad \|S(\cdot,t)+I(\cdot,t)\|_{L^1(\Omega)} = \|S_0+I_0\|_{L^1(\Omega)}, \tag{15}
$$

providing a uniform L^1 bound for all $t\in[0,T]$. Then, we define the total population density variable $N(x,t) = S(x,t)+I(x,t)$ to establish the necessary a priori estimates, dividing the analysis into two cases based on the diffusion parameters: $d_S = d_I = \hat{d}$ and $d_S \neq d_I$.

Case (a): Let $d_S = d_I = \hat{d}$. In this case (12)–(13), implies that N satisfies a linear heat equation subject to homogeneous Neumann boundary conditions

$$
N_t - \hat{d}\Delta N = 0 \quad \text{in } Q_T, \quad \text{with} \quad \nabla N\cdot\boldsymbol{\eta} = 0 \quad \text{on } \Gamma.
$$

By the standard parabolic maximum principle, the total population density is uniformly bounded in time by the initial populations, which directly implies:

$$
0 \le S(x,t), I(x,t) \le N(x,t) \le \|S_0+I_0\|_{L^\infty(\Omega)} < \infty, \quad \forall (x,t)\in\overline{Q}_T.
$$

Consequently, the uniform estimate (11) holds immediately for this case, without requiring any further global growth condition on assumption (A3).

Case (b): Let $d_S \neq d_I$. From (12), we deduce that $N(x,t)$ satisfy the parabolic relation

$$
N_t - d_I\Delta N = (d_S - d_I)\Delta S \quad \text{in } Q_T. \tag{16}
$$

Multiplying (16) by $N(x,t)$, integrating by parts over the bounded spatial domain Ω, utilizing the boundary conditions (5), and applying the ϵ–Young's inequality with $\epsilon = d_I$, we deduce:

$$
\frac{1}{2}\frac{\mathrm{d}}{\mathrm{d}t}\int_\Omega N^2 dx + \frac{d_I}{2}\int_\Omega |\nabla N|^2 dx \le \frac{(d_S-d_I)^2}{2d_I}\int_\Omega |\nabla S|^2 \mathrm{d}x. \tag{17}
$$

Moreover, multiplying the first state equation (3) by S, and using the fact that the generalized non-linear incidence function satisfies $f(S, I) \geq 0$ for all $(S, I) \in \mathbb{R}_+^2$ assumed in Assumption (A3), Assumption (A4), and $0 \leq I \leq N$, we get the inequality:

$$\begin{aligned}\frac{1}{2}\frac{\mathrm{d}}{\mathrm{d}t}\int_\Omega S^2 dx + d_S \int_\Omega |\nabla S|^2 dx &\leq \gamma^\top \int_\Omega SI dx \\ &\leq \frac{\gamma^\top}{2}\int_\Omega S^2 \mathrm{d}x + \frac{\gamma^\top}{2}\int_\Omega N^2 dx. \qquad (18)\end{aligned}$$

Multiplying (18) by $\xi > (d_S - d_I)^2/2d_S d_I$ and adding the result to (17), we obtain the following coupled energy estimate:

$$\begin{aligned}\frac{1}{2}\frac{\mathrm{d}}{\mathrm{d}t}\int_\Omega (\xi S^2 + N^2)\, dx + \left(\xi d_S - \frac{(d_S - d_I)^2}{2d_I}\right)\int_\Omega |\nabla S|^2\, dx + \frac{d_I}{2}\int_\Omega |\nabla N|^2\, dx \\ \leq \max\left\{\frac{\gamma^\top}{2}, \frac{\xi\gamma^\top}{2}\right\}\int_\Omega (\xi S^2 + N^2)\, dx. \qquad (19)\end{aligned}$$

where the choice of ξ guarantees that the coefficient of the second term on left hand side remains strictly positive. Applying the Grönwall's inequality over $[0, t]$, we conclude the following estimate

$$\int_\Omega (\xi S^2(t) + N^2(t))\, \mathrm{d}x \leq \left(\int_\Omega (\xi S^2(0) + N^2(0))\, \mathrm{d}x\right) e^{\kappa t}, \quad \forall t \in [0, T]. \quad (20)$$

with $\kappa = \gamma^\top \max\{\xi, 1/\xi\}$.

From the energy estimate (20) and using the fact that $N(x, t)$ bounds the infected population $I(x, t)$, it follows immediately that there exists a positive constant M_0, depending only on the initial data, such that the $L^2(\Omega)$-norms of the biological components are uniformly bounded for all time, i.e.,

$$\|S(\cdot, t)\|_{L^2(\Omega)} + \|I(\cdot, t)\|_{L^2(\Omega)} \leq M_0, \quad \forall t \in (0, \infty).$$

In order to lift these L^2-bounds to the $L^\infty(\Omega)$-norm, we apply the result given in [36, Lemma 2.1]. We observe that all the required conditions of that lemma are satisfied: the components possess uniform bounds in $L^{p_0}(\Omega)$ with $p_0 = 2$; the non-linear incidence function satisfies the polynomial growth condition with exponent q; and for a spatial dimension $n \leq 3$, the sub-criticality condition $\max\{0, q-1\} < \frac{4}{n}$ holds strictly since $\max\{0, 1\} = 1 < \frac{4}{3}$. Consequently, by virtue of [36, Lemma 2.1], we obtain the uniform $L^\infty(\Omega)$ bounds given in (11). $\square$

Theorem 1. *Suppose that the assumptions (A1)-(A4) are satisfied and consider the notation $\mathcal{W}(0,T)$ for the reflexive Banach space:*

$$\mathcal{W}(0,T) = \Big\{u \in L^2(0,T;H^1(\Omega)) : \partial_t u \in L^2(0,T;H^{-1}(\Omega))\Big\}, \qquad (21)$$

equipped with the norm $\|u\|_{\mathcal{W}} = \|u\|_{L^2(0,T;H^1)} + \|\partial_t u\|_{L^2(0,T;H^{-1})}$. Then, the initial boundary value problem (3)-(6) admits a unique global classical solution (S,I) such that:

$$(S,I) \in [C^{2+\alpha,1+\alpha/2}(\overline{Q}_T)]^2, \qquad (22)$$

$$S(x,t) \geq 0 \text{ and } I(x,t) \geq 0 \text{ on } \overline{Q}_T, \qquad (23)$$

$$\|(S+I)(\cdot,t)\|_{L^1(\Omega)} = \|S_0 + I_0\|_{L^1(\Omega)}, \text{ for all } t \geq 0, \qquad (24)$$

$$\|S(\cdot,t)\|_{L^\infty(\Omega)} + \|I(\cdot,t)\|_{L^\infty(\Omega)} \leq C, \text{ for all } t \geq 0, \qquad (25)$$

$$\|S\|_{\mathcal{W}(0,T)} + \|I\|_{\mathcal{W}(0,T)} \leq C, \qquad (26)$$

for a constant $C > 0$, depending only on Ω, T, d_S, d_I, and the initial data (S_0, I_0). In particular, the mapping $t \mapsto (S(\cdot,t), I(\cdot,t))$ is continuous from $[0,T]$ into $[L^2(\Omega)]^2$.

Proof. We first establish the existence and uniqueness of local solutions, and subsequently extend these results to ensure global well-posedness.

To prove the local existence and uniqueness of the solution for the system (3)–(6), we apply the classical Schauder theory for semilinear parabolic equations [20, 21]. It can be summarized as follows. Let us consider $M > 0$, a constant determined by the initial data, and $T^* > 0$ be a sufficiently small time horizon, we define the closed and convex set X as follows:

$$X = \Big\{(S,I) \in [C^{\alpha,\alpha/2}(\overline{Q}_{T^*})]^2 : (S,I)(\cdot,0) = (S_0,I_0),\ \|(S,I)\|_{C^{\alpha,\alpha/2}} \leq M\Big\}.$$

We introduce the linearization operator $\mathcal{T}$ from X to $[C^{2+\alpha,1+\alpha/2}(\overline{Q}_{T^*})]^2$, such that for any $(\hat{S},\hat{I}) \in X$, the pair $(S,I) = \mathcal{T}(\hat{S},\hat{I})$ is defined as the unique solution to the linearized system:

$$S_t - d_S \Delta S = -\beta(x,t) f(\hat{S},\hat{I}) + \gamma(x,t)\hat{I}, \qquad \text{in } Q_{T^*}, \qquad (27)$$

$$I_t - d_I \Delta I = \beta(x,t) f(\hat{S},\hat{I}) - \gamma(x,t)\hat{I}, \qquad \text{in } Q_{T^*}, \qquad (28)$$

$$\nabla S \cdot \boldsymbol{\eta} = \nabla I \cdot \boldsymbol{\eta} = 0, \qquad \text{on } \Gamma^*, \qquad (29)$$

$$(S,I)(x,0) = (S_0,I_0)(x), \qquad \text{in } \Omega. \qquad (30)$$

We notice that the Hölder continuity of the source term as consequence of the assumptions (A3), (A4) and the definition of the set X, or more specifically, if $\hat{S}, \hat{I} \in C^{\alpha,\alpha/2}(\overline{Q}_T)$ and $f \in C^{1+\alpha}_{loc}([0,\infty)^2)$ then reaction terms have the regularity $\mp\beta f(\hat{S},\hat{I}) \pm \gamma\hat{I} \in C^{\alpha,\alpha/2}(\overline{Q}_T)$. According to the linear Schauder theory [20, 21], there exists a unique solution (S,I) of (27)-(30) satisfying the estimate:

$$
\begin{aligned}
&\|(S,I)\|_{[C^{2+\alpha,1+\alpha/2}(\overline{Q}_{T^*})]^2} \\
&\le C\left(\left\|\Big(-\beta f(\hat{S},\hat{I}) + \gamma\hat{I}, \beta f(\hat{S},\hat{I}) - \gamma\hat{I}\Big)\right\|_{[C^{\alpha,\alpha/2}(\overline{Q}_{T^*})]^2}\right. \\
&\qquad\qquad \left. + \left\|(S_0,I_0)\right\|_{[C^{2+\alpha}(\overline{\Omega})]^2}\right).
\end{aligned}
$$

Hence, by the fixed point arguments, we follow the existence of local solutions. For a sufficiently small T^*, the mapping $\mathcal{T}$ satisfies $\mathcal{T}(X) \subseteq X$. Using the fact that the embedding $C^{2+\alpha,1+\alpha/2} \hookrightarrow C^{\alpha,\alpha/2}$ is compact by the Arzelà-Ascoli Theorem, we deduce that $\mathcal{T}$ is a compact operator. Then, by Schauder's Fixed-Point Theorem, there exists at least one point $(\bar{S},\bar{I}) \in X$ such that $\mathcal{T}(\bar{S},\bar{I}) = (\bar{S},\bar{I})$, which constitutes a classical local solution. Moreover, the uniqueness of the solution in $[0,T^*]$ follows from the C^1 regularity of f, which implies it is locally Lipschitz. If two solutions were to exist, their difference would satisfy a linear system with zero initial data. By applying Gronwall's inequality to the L^2-norm of the difference, we conclude that the solutions must coincide identically on $\overline{Q}_{T^*}$.

The transition from local existence to global existence is established by showing that the classical solution (S,I) does not blow up in any finite time interval $[0,T_{\max}]$. This is achieved through uniform a priori estimates. From (A3) we have that $f(S,I) > 0$, $f(0,0) = f(0,I) = f(S,0) = 0$ for $(S,I) \in \mathbb{R}^2_+$, and we can deduce that $(0,0)$ is a sub-solution of (3)–(6) on $Q_{T_{\max}}$. Then, the assumption (A2) and the parabolic comparison principle implies that $S(x,t) \ge 0$ and $I(x,t) \ge 0$ on $Q_{T_{\max}}$. Proceeding as (12)–(14) we get a uniform L^1 bound for all $t \in [0,T]$, and particularly on $[0,T_{\max}]$. Moreover, by application of Lemma 1 we get the the uniform $L^\infty(\Omega)$ estimate, which implies that the local solution provided by Schauder's Theory can be uniquely extended to the entire interval $[0,T_{\max}]$ for any $T_{\max} > 0$. We thus conclude that $T_{max} = \infty$ and clearly the solution satisfies the regularity (22) and the estimates given in (23)-(25).

The estimate in (26) is derived by energy estimates: testing the equations with (S, I), applying Green's identity, replacing the Neumann boundary conditions, and then using the Gronwall's inequality. The trace result is a classical result for functions in $\mathcal{W}(0,T)$ and the fact that the state variables (S, I) belong to the Hölder space $[C^{2+\alpha,1+\alpha/2}(\overline{Q}_T)]^2$, regularity that implies the trace at any time $t \in [0, T]$ is well-defined in the classical sense as an element of $[C^{2+\alpha}(\overline{\Omega})]^2$. □

2.2. Coefficient stability of the state system solution.

Theorem 2. *Suppose that the assumptions (A1)-(A4) are satisfied and consider that (S, I) and $(\hat{S}, \hat{I})$ are solutions to (3)-(6) with coefficients (β, γ) and $(\hat{\beta}, \hat{\gamma})$ belonging to $\mathcal{U}_{ad}$, respectively. Then, the estimate*

$$\|((\hat{S}, \hat{I}) - (S, I))(\cdot, t)\|^2_{[L^2(\Omega)]^2} \leq C\|(\hat{\beta}, \hat{\gamma}) - (\beta, \gamma)\|^2_{[L^2(Q_T)]^2}, \tag{31}$$

holds for any $t \in [0, T]$ and C a positive constant.

Proof. Let us define the error of the states as $s = \hat{S} - S$, $i = \hat{I} - I$, and the control perturbations as $\delta\beta = \hat{\beta} - \beta$, $\delta\gamma = \hat{\gamma} - \gamma$. Subtracting the corresponding equations for (S, I) and $(\hat{S}, \hat{I})$, we obtain the following system for (s, i):

$$s_t - d_S\Delta s = -[\hat{\beta} f(\hat{S}, \hat{I}) - \beta f(S, I)] + (\hat{\gamma}\hat{I} - \gamma I), \qquad \text{in } Q_T, \tag{32}$$

$$i_t - d_I\Delta i = [\hat{\beta} f(\hat{S}, \hat{I}) - \beta f(S, I)] - (\hat{\gamma}\hat{I} - \gamma I), \qquad \text{in } Q_T, \tag{33}$$

$$\nabla s \cdot \boldsymbol{\eta} = \nabla i \cdot \boldsymbol{\eta} = 0, \qquad \text{on } \Gamma, \tag{34}$$

$$(s, i)(x, 0) = 0, \qquad \text{in } \Omega. \tag{35}$$

We decompose and bound the non-linear and linear terms on the reaction, by using the Assumption (A3) and the fact that the states are bounded (see Theorem 1):

$$\begin{aligned}|\hat{\beta} f(\hat{S}, \hat{I}) - \beta f(S, I)| &= |\delta\beta f(\hat{S}, \hat{I}) + \beta(f(\hat{S}, \hat{I}) - f(S, I))| \\ &\leq C(|\delta\beta| + |s| + |i|),\end{aligned} \tag{36}$$

$$|\hat{\gamma}\hat{I} - \gamma I| = |\delta\gamma\hat{I} + \gamma i| \leq C(|\delta\gamma| + |i|), \tag{37}$$

where C depends on the L^∞-bounds of the states and the Lipschitz constant of f. Multiplying (32) and (33) by s and i respectively, integrating over Ω, and applying the boundary conditions, we have

$$\frac{1}{2}\frac{d}{dt}\|s(\cdot, t)\|^2_{L^2} + d_S\|\nabla s(\cdot, t)\|^2_{L^2} \leq \int_\Omega |\hat{\beta} f(\hat{S}, \hat{I}) - \beta f(S, I)||s|(x, t)dx,$$

$$\frac{1}{2}\frac{d}{dt}\|i(\cdot,t)\|_{L^2}^2 + d_I\|\nabla i(\cdot,t)\|_{L^2}^2 \le \int_\Omega |\hat{\beta}f(\hat{S},\hat{I}) - \beta f(S,I)||i|(x,t)dx \\ + \int_\Omega |\hat{\gamma}\hat{I} - \gamma I||i|(x,t)dx.$$

Using the bounds (36)–(37), the Young's inequality, and summing both resulting inequalities, we get

$$\frac{d}{dt}\left(\|s(\cdot,t)\|_{L^2}^2 + \|i(\cdot,t)\|_{L^2}^2\right) \\ \le C\Big\{\|s(\cdot,t)\|_{L^2}^2 + \|i(\cdot,t)\|_{L^2}^2 + \|\delta\beta(\cdot,t)\|_{L^2}^2 + \|\delta\gamma(\cdot,t)\|_{L^2}^2\Big\}.$$

Consequently, by applying the Gronwall inequality we obtain

$$\|s(\cdot,t)\|_{L^2}^2 + \|i(\cdot,t)\|_{L^2}^2 \le C\int_0^T \left(\|\delta\beta(\cdot,\tau)\|_{L^2}^2 + \|\delta\gamma(\cdot,\tau)\|_{L^2}^2\right)d\tau.$$

This concludes the proof of the desired estimate (31). □

3. Analysis and Results of the Optimal Control Problem.

3.1. Existence of Solutions of the Optimal Control Problem

Theorem 3. *Suppose that the assumptions (A1)-(A5) are satisfied. There exists at least one solution to the optimization problem* (10)*.*

Proof. We prove the result by using the standard direct method of the calculus of variations, constructing minimizing sequences, and utilizing appropriate compactness embeddings.

We begin by noticing that $\mathcal{U}_{ad}$ is non-empty, and the cost functional $J(S,I)$ is bounded from below since $J \ge 0$. Thus, there exists a minimizing sequence $\{(\beta_n,\gamma_n)\}_{n=1}^\infty \subset \mathcal{U}_{ad}$ such that:

$$\lim_{n\to\infty}\mathcal{J}(\beta_n,\gamma_n) = \inf_{(\beta,\gamma)\in\mathcal{U}_{ad}}\mathcal{J}(\beta,\gamma).$$

The set $\mathcal{U}_{ad}$ is a closed, bounded, and convex subset of $[C^{\alpha,\alpha/2}(\overline{Q}_T)]^2 \cap [L^2(0,T;H^1(\Omega))]^2$. Its uniform Hölder bound and the Arzelà–Ascoli theorem give compactness in $[C(\overline{Q}_T)]^2$, while the $L^2(0,T;H^1(\Omega))$ bound gives weak compactness in the spatial Sobolev topology. Therefore, we can extract a subsequence (still denoted by $\{(\beta_n,\gamma_n)\}_{n=1}^\infty$) and a limit pair $(\bar{\beta},\bar{\gamma}) \in \mathcal{U}_{ad}$

such that $(\beta_n, \gamma_n) \to (\bar{\beta}, \bar{\gamma})$ uniformly in $\overline{Q}_T$, and $(\beta_n, \gamma_n) \rightharpoonup (\bar{\beta}, \bar{\gamma})$ weakly in $[L^2(0, T; H^1(\Omega))]^2$.

Let (S_n, I_n) be the unique classical solution of the state system associated with (β_n, γ_n) for each $n \in \mathbb{N}$. From Theorem 1, the sequence $\{(S_n, I_n)\}_{n=1}^{\infty}$ is uniformly bounded in the Hölder space $[C^{2+\alpha,1+\alpha/2}(\overline{Q}_T)]^2$. By the compactness of the embedding $[C^{2+\alpha,1+\alpha/2}(\overline{Q}_T)]^2 \hookrightarrow [C^{2,1}(\overline{Q}_T)]^2 \hookrightarrow [C(\overline{Q}_T)]^2$ via the Arzelà–Ascoli Theorem, we can extract a subsequence such that $(S_n, I_n) \to (\bar{S}, \bar{I})$ uniformly in $\overline{Q}_T$. This uniform convergence guarantees, in particular, the strong convergence of the state variables at the final time, i.e., $(S_n, I_n)(\cdot, T) \to (\bar{S}, \bar{I})(\cdot, T)$ strongly in $[L^2(\Omega)]^2$. Additionally, from the energy bounds (26) and the Aubin–Lions Lemma, the sequence is uniformly bounded in $[\mathcal{W}(0, T)]^2$, ensuring that $\partial_t S_n \rightharpoonup \partial_t \bar{S}$ and $\partial_t I_n \rightharpoonup \partial_t \bar{I}$ weakly in $L^2(0, T; H^{-1}(\Omega))$.

The strong convergence of the sequence of the states $\{(S_n, I_n)\}_{n=1}^{\infty}$, combined with the uniform convergence of the sequence of controls $\{(\beta_n, \gamma_n)\}_{n=1}^{\infty}$, allows us to pass to the limit in the coupled non-linear terms. Specifically, as $n \to \infty$, we have that $\beta_n f(S_n, I_n) \to \bar{\beta} f(\bar{S}, \bar{I})$ and $\gamma_n I_n \to \bar{\gamma}\bar{I}$ strongly in $L^2(Q_T)$ (and almost everywhere in Q_T). This convergence is justified by the continuity of f and the fact that the product of a uniformly convergent sequence and a strongly L^2-convergent sequence converges strongly in L^2. Consequently, we verify that the limit $(\bar{S}, \bar{I})$ is indeed the classical solution associated with the optimal control $(\bar{\beta}, \bar{\gamma})$.

The norm in L^2 is weakly lower semicontinuous. Specifically, for the regularization term:

$$\|\nabla_x(\bar{\beta}, \bar{\gamma})\|^2_{[L^2(Q_T)]^{2d}} \leq \liminf_{n\to\infty} \|\nabla_x(\beta_n, \gamma_n)\|^2_{[L^2(Q_T)]^{2d}}.$$

Combining this property with the strong convergence of the states in $[L^2(\Omega)]^2$ at $t = T$, we deduce that $\mathcal{J}(\bar{\beta}, \bar{\gamma}) \leq \liminf_{n\to\infty} \mathcal{J}(\beta_n, \gamma_n)$. Since $(\bar{\beta}, \bar{\gamma}) \in \mathcal{U}_{ad}$, it achieves the minimum value of the reduced cost functional. Hence, $(\bar{\beta}, \bar{\gamma})$ constitutes an optimal control solution to problem (10), which completes the proof of the theorem. □

3.2. Well-posedness and Coefficient-observations Stability of the Adjoint System.

The adjoint system for (3)–(6) can be derived using the Lagrange multiplier method. For the optimal control problem (10), we define the Lagrangian functional $\mathcal{L} = \mathcal{L}(S, I, \beta, \gamma, p_1, p_2)$ as follows:

$$\begin{aligned}
\mathcal{L} = J(S,I) - \iint_{Q_T} p_1 \left(\partial_t S - d_S \Delta S + \beta f(S,I) - \gamma I\right) dxdt \\
- \iint_{Q_T} p_2 \left(\partial_t I - d_I \Delta I - \beta f(S,I) + \gamma I\right) dxdt \\
= J(S,I) + \iint_{Q_T} \Big\{ S(\partial_t p_1 + d_S \Delta p_1) + I(\partial_t p_2 + d_I \Delta p_2) \\
+ (\beta f(S,I) - \gamma I)(p_2 - p_1) \Big\} dxdt \\
- \int_\Omega (p_1 S + p_2 I)(x,T) dx + \int_\Omega (p_1(x,0) S_0(x) + p_2(x,0) I_0(x)) dx \\
- \int_\Gamma \Big(d_S S \nabla p_1 \cdot \boldsymbol{\eta} + d_I I \nabla p_2 \cdot \boldsymbol{\eta} \Big) dSdt.
\end{aligned} \tag{38}$$

The necessary condition to satisfy $\nabla_{(S,I)} \mathcal{L} = 0$ is obtained by vanishing the first variation of $\mathcal{L}$ with respect to the state variables S and I, evaluated at $(\overline{S}, \overline{I})$, which is the unique classical solution of (3)–(6) associated with the optimal pair $(\overline{\beta}, \overline{\gamma}) \in \mathcal{U}_{ad}$. This optimization requirement implies that the Lagrange multipliers (p_1, p_2) must solve the backward-in-time system:

$$-(p_1)_t - d_S \Delta p_1 = \overline{\beta}(x,t) \partial_1 f(\overline{S}, \overline{I})(p_2 - p_1), \qquad \text{in } Q_T, \tag{39}$$

$$-(p_2)_t - d_I \Delta p_2 = \Big(\overline{\beta}(x,t) \partial_2 f(\overline{S}, \overline{I}) - \overline{\gamma}(x,t) \Big)(p_2 - p_1), \qquad \text{in } Q_T, \tag{40}$$

$$\nabla p_1 \cdot \boldsymbol{\eta} = \nabla p_2 \cdot \boldsymbol{\eta} = 0, \qquad \text{on } \Gamma, \tag{41}$$

$$(p_1, p_2)(x,T) = (\overline{S}, \overline{I})(x,T) - (S^{obs}, I^{obs})(x), \qquad \text{in } \Omega. \tag{42}$$

It is called the the adjoint system to the state system (3)-(6).

Theorem 4. *Suppose that the assumptions (A1)-(A5) are satisfied and consider the notation $(\overline{S}, \overline{I})$ for the strong solution of (3)-(6) associated with $(\overline{\beta}, \overline{\gamma}) \in \mathcal{U}_{ad}$ a solution of (10). Then, there exists a unique classical solution $(p_1, p_2) \in [C^{2+\alpha, 1+\alpha/2}(\overline{Q}_T)]^2$ to the backward-boundary value problem (39)-(42). Moreover, the following uniform estimates hold:*

$$\|(p_1, p_2)\|_{[C^{2+\alpha,1+\alpha/2}(\overline{Q}_T)]^2} \leq C \|(\bar{S} - S^{obs}, \bar{I} - I^{obs})\|_{[C^{2+\alpha}(\overline{\Omega})]^2}, \tag{43}$$

$$\|(p_1, p_2)(\cdot, t)\|^2_{[L^2(\Omega)]^2} \leq C, \ \textit{for } t \in [0,T], \tag{44}$$

$$\|(p_1, p_2)(\cdot, t)\|^2_{[H^1(\Omega)]^2} \leq C, \ \textit{for } t \in [0,T], \tag{45}$$

$$\|\Delta(p_1,p_2)(\cdot,t)\|^2_{[L^2(\Omega)]^2} \leq C, \ \textit{for } t \in [0,T], \tag{46}$$
$$\|(p_1,p_2)(\cdot,t)\|^2_{[L^\infty(\Omega)]^2} \leq C, \ \textit{for } t \in [0,T], \tag{47}$$

for a positive constant C independent of $(\overline{\beta},\overline{\gamma})$.

Proof. We rewrite the end backward-boundary problem (39)-(42) as the following initial-boundary value problem

$$(q_1)_\tau - d_S\Delta q_1 = \beta^*(x,\tau)\partial_1 f(S^*,I^*)(q_2-q_1), \quad \text{in } Q_T, \tag{48}$$
$$(q_2)_\tau - d_I\Delta q_2 = (\beta^*(x,\tau)\partial_2 f(S^*,I^*) - \gamma^*(x,\tau))(q_2-q_1), \quad \text{in } Q_T, \tag{49}$$
$$\nabla q_1 \cdot \boldsymbol{\eta} = \nabla q_2 \cdot \boldsymbol{\eta} = 0, \quad \text{on } \Gamma, \tag{50}$$
$$(q_1,q_2)(x,0) = (\bar{S}-S^{obs}, \bar{I}-I^{obs})(x) \quad \text{in } \Omega. \tag{51}$$

by considering $\tau = T-t$ for $t \in [0,T]$, $(q_1,q_2)(x,\tau) = (p_1,p_2)(x,T-\tau)$, $(S^*,I^*)(x,\tau) = (\overline{S},\overline{I})(x,T-\tau)$, and $(\beta^*,\gamma^*)(x,\tau) = (\overline{\beta},\overline{\gamma})(x,T-\tau)$. We notice that the system (48)-(51) is linear with all coefficients belong to $C^{\alpha,\alpha/2}(\overline{Q}_T)$, and the initial condition has the regularity $C^{2+\alpha}(\overline{\Omega})$. Then the existence and uniqueness of a classical solution $(q_1,q_2) \in [C^{2+\alpha,1+\alpha/2}(\overline{Q}_T)]^2$ follows from the standard linear Schauder theory [20, 21]. Additionally, from the Schauder estimate, we get that the inequality

$$\|(q_1,q_2)\|_{[C^{2+\alpha,1+\alpha/2}(\overline{Q}_T)]^2} \leq C\|(\bar{S}-S^{obs}, \bar{I}-I^{obs})\|_{[C^{2+\alpha}(\overline{\Omega})]^2},$$

is satisfied. Then, we deduce (43) and the other estimates are a consequence of the fact that Schauder regularity is stronger than the Sobolev norms mentioned or a bound in $C^{2+\alpha}$ automatically ensures uniform-in-time control over the other spatial norms. More precisely, we have that (44) is deduced from the fact that $(p_1,p_2)(\cdot,t)$ is continuous on the bounded domain Ω; (45) is a consequence of (44) and the fact that $\nabla(p_1,p_2)(\cdot,t)L^2(\Omega)$ is bounded since $(p_1,p_2)(\cdot,t) \in [C^2(\overline{\Omega})]^2$, its first derivatives $\nabla(p_1,p_2)(\cdot,t)$ are continuous and bounded; (46) is satisfied since $\Delta p(p_1,p_2)(\cdot,t)$ is continuous on $\overline{\Omega}$ and L^2 norm is necessarily bounded; and (47) is an immediate consequence of the definition of the Hölder norm, since we have that $\|(p_1,p_2)(\cdot,t)\|_{[L^\infty(\Omega)]^2} \leq \|(p_1,p_2)(\cdot,t)\|_{[C^{2+\alpha}(\overline{Q}_T)]^2}$. □

Theorem 5. *Suppose that the assumptions Theorem 2 are satisfied and consider the adjoint states (p_1,p_2) and $(\hat{p}_1,\hat{p}_2)$ are solutions to (39)-(42) with controls (β,γ) and $(\hat{\beta},\hat{\gamma})$ and observations (S^{obs},I^{obs}) and $(\hat{S}^{obs},\hat{I}^{obs})$, respectively. Then, the estimates*

$$\|((\hat{p}_1,\hat{p}_2)-(p_1,p_2))(\cdot,t)\|^2_{[L^2(\Omega)]^2}$$

$$\leq C\left(\|(\hat{\beta},\hat{\gamma})-(\beta,\gamma)\|^2_{[L^2(Q_T)]^2}+\|(\hat{S}^{obs},\hat{I}^{obs})-(S^{obs},I^{obs})\|^2_{[L^2(\Omega)]^2}\right), \quad (52)$$

holds for any $t \in [0,T]$ and C a positive constant.

Proof. The result is established by a similar argument to that of Theorem 2. By defining the adjoint errors as $P_1 = \hat{p}_1 - p_1$ and $P_2 = \hat{p}_2 - p_2$, writing their corresponding system, and testing the equations with (P_1, P_2), we can develop the standard energy estimates. Applying the assumption of the local Lipschitz continuity of the derivatives of f, the uniform bounds of the states from Theorem 1, and integrating backwards from $t = T$, and using Gronwall's inequality we get the stability estimate (52). □

3.3. First order optimality condition(3)-(6)

Theorem 6. *Suppose that the assumptions of Theorem 4 are satisfied. Then, the inequality*

$$\begin{aligned}\iint_{Q_T}\Big\{&\Big[(\hat{\beta}-\overline{\beta})f(\overline{S},\overline{I})-(\hat{\gamma}-\overline{\gamma})\overline{I}\Big](p_2-p_1)\\&+\Lambda\nabla_x\overline{\beta}\cdot\nabla_x\Big(\hat{\beta}-\overline{\beta}\Big)+\Lambda\nabla_x\overline{\gamma}\cdot\nabla_x\Big(\hat{\gamma}-\overline{\gamma}\Big)\Big\}dxdt\geq 0,\end{aligned} \quad (53)$$

is satisfied for any $(\hat{\beta},\hat{\gamma}) \in \mathcal{U}_{ad}$. In particular, if $(\overline{\beta},\overline{\gamma})$ belongs to the interior of $\mathcal{U}_{ad}$ so that arbitrary signed variations are admissible, then the optimal controls satisfy the following system of elliptic equations with natural homogeneous Neumann boundary conditions:

$$-\Lambda\Delta_x\overline{\beta} = -f(\overline{S},\overline{I})(p_2-p_1), \qquad \text{in } Q_T, \quad (54)$$

$$-\Lambda\Delta_x\overline{\gamma} = \overline{I}(p_2-p_1), \qquad \text{in } Q_T, \quad (55)$$

subject to the boundary conditions $\nabla_x\overline{\beta}\cdot\boldsymbol{\eta} = \nabla_x\overline{\gamma}\cdot\boldsymbol{\eta} = 0$ on Γ.

Proof. Let $(\hat{\beta},\hat{\gamma}) \in \mathcal{U}_{ad}$ be arbitrary. Since $\mathcal{U}_{ad}$ is convex, the convex combination $(\beta^\epsilon,\gamma^\epsilon) = (1-\epsilon)(\bar{\beta},\bar{\gamma}) + \epsilon(\hat{\beta},\hat{\gamma})$ also belongs to $\mathcal{U}_{ad}$ for any $\epsilon \in [0,1]$. Let (S^ϵ, I^ϵ) and $(\bar{S},\bar{I})$ be the solutions to (3)–(6) corresponding to the controls $(\beta^\epsilon,\gamma^\epsilon)$ and $(\bar{\beta},\bar{\gamma})$, respectively. For convenience, we adopt the following notation:

$$(z_1^\epsilon, z_2^\epsilon) = \left(\frac{S^\epsilon-\overline{S}}{\epsilon}, \frac{I^\epsilon-\overline{I}}{\epsilon}\right), \quad (z_1,z_2) = \lim_{\epsilon\to 0}(z_1^\epsilon, z_2^\epsilon),$$

$$
\begin{aligned}
F^\epsilon &= -\beta^\epsilon \left\{ \left[\frac{f(S^\epsilon, I^\epsilon) - f(\overline{S}, I^\epsilon)}{S^\epsilon - \overline{S}} \right] z_1^\epsilon + \left[\frac{f(\overline{S}, I^\epsilon) - f(\overline{S}, \overline{I})}{I^\epsilon - \overline{I}} \right] z_2^\epsilon \right\} \\
&\quad - (\hat{\beta} - \overline{\beta}) f(\overline{S}, \overline{I}) + \gamma^\epsilon z_2^\epsilon + (\hat{\gamma} - \overline{\gamma}) \overline{I}, \\
F &= -\overline{\beta} \Big(\partial_1 f(\overline{S}, \overline{I}) z_1 + \partial_2 f(\overline{S}, \overline{I}) z_2 \Big) - (\hat{\beta} - \overline{\beta}) f(\overline{S}, \overline{I}) + \overline{\gamma} z_2 + (\hat{\gamma} - \overline{\gamma}) \overline{I}.
\end{aligned}
$$

The sensitivity variables $(z_1^\epsilon, z_2^\epsilon)$ converge uniformly to (z_1, z_2) (due to Schauder estimates and Theorem 2) and the perturbed controls $(\beta^\epsilon, \gamma^\epsilon)$ converge uniformly to $(\bar{\beta}, \bar{\gamma})$. Furthermore, we notice that $F^\epsilon \to F$ as $\epsilon \to 0$, which is established by using the regularity of the incidence function f and the properties of the states (S^ϵ, I^ϵ) and $(\bar{S}, \bar{I})$ given in Theorem 1. Specifically, since $f \in C^{1+\alpha}_{loc}([0,\infty)^2)$ by Assumption (A3), the terms in square brackets in F^ϵ are difference quotients that, by the mean value theorem, satisfy:

$$
\begin{aligned}
\frac{f(S^\epsilon, I^\epsilon) - f(\bar{S}, I^\epsilon)}{S^\epsilon - \bar{S}} &= \partial_1 f(\xi^\epsilon, I^\epsilon), \quad \text{with } \xi^\epsilon \in (\bar{S}, S^\epsilon), \\
\frac{f(\bar{S}, I^\epsilon) - f(\bar{S}, \bar{I})}{I^\epsilon - \bar{I}} &= \partial_2 f(\bar{S}, \eta^\epsilon), \quad \text{with } \eta^\epsilon \in (\bar{I}, I^\epsilon).
\end{aligned}
$$

Consequently, the continuity of the partial derivatives $\partial_1 f$ and $\partial_2 f$ implies that $\partial_1 f(\xi^\epsilon, I^\epsilon)$ and $\partial_2 f(\bar{S}, \eta^\epsilon)$ converge to $\partial_1 f(\bar{S}, \bar{I})$ and $\partial_2 f(\bar{S}, \bar{I})$, respectively.

Subtracting the systems for the states (S^ϵ, I^ϵ) and $(\bar{S}, \bar{I})$, and subsequently dividing by ϵ, we deduce that $(z_1^\epsilon, z_2^\epsilon)$ satisfies the system

$$
\begin{aligned}
(z_1^\epsilon)_t - d_S \Delta z_1^\epsilon &= F^\epsilon, && \text{in } Q_T, && (56) \\
(z_2^\epsilon)_t - d_I \Delta z_2^\epsilon &= -F^\epsilon, && \text{in } Q_T, && (57) \\
\nabla z_1^\epsilon \cdot \boldsymbol{\eta} = \nabla z_2^\epsilon \cdot \boldsymbol{\eta} &= 0, && \text{on } \Gamma, && (58) \\
(z_1^\epsilon, z_2^\epsilon)(x, 0) &= 0, && \text{in } \Omega. && (59)
\end{aligned}
$$

Then, taking the limit as $\epsilon \to 0^+$ in (56)-(59), we have that (z_1, z_2) is solution of the system

$$
\begin{aligned}
(z_1)_t - d_S \Delta z_1 &= F, && \text{in } Q_T, && (60) \\
(z_2)_t - d_I \Delta z_2 &= -F, && \text{in } Q_T, && (61) \\
\nabla z_1 \cdot \boldsymbol{\eta} = \nabla z_2 \cdot \boldsymbol{\eta} &= 0, && \text{on } \Gamma, && (62) \\
(z_1, z_2)(x, 0) &= (0, 0), && \text{in } \Omega. && (63)
\end{aligned}
$$

The well-posedness of the systems (56)–(59) and (60)–(63) follows from Schauder theory, since the initial conditions and the reaction terms satisfy the required Hölder regularity.

Let $\mathcal{J}_\epsilon$ be the evaluation of $\mathcal{J}$ at $(\beta^\epsilon, \gamma^\epsilon)$, i. e,

$$\mathcal{J}_\epsilon = \frac{1}{2}\|(S^\epsilon, I^\epsilon)(\cdot, T) - (S^{obs}, I^{obs})\|^2_{[L^2(\Omega)]^2} + \frac{\Lambda}{2}\|\nabla(\beta^\epsilon, \gamma^\epsilon)\|^2_{[L^2(Q_T)]^2}.$$

From the definition of (S^ϵ, I^ϵ) and using the hypothesis that $(\overline{\beta}, \overline{\gamma})$ is a solution of (10), we follow that

$$\begin{aligned}
\frac{dJ_\epsilon}{d\epsilon}\Big|_{\epsilon=0} &= \int_\Omega \Big(S^\epsilon(x,T) - S^{obs}(x)\Big)\frac{\partial}{\partial\epsilon}S^\epsilon(x,T) + \Big(I^\epsilon(x,T) - I^{obs}(x)\Big) \\
&\qquad \times \frac{\partial}{\partial\epsilon}I^\epsilon(x,T)dx\Big|_{\epsilon=0} + \Lambda\iint_{Q_T}\nabla(\overline{\beta}, \overline{\gamma})\cdot\nabla\Big((\hat{\beta}, \hat{\gamma}) - (\overline{\beta}, \overline{\gamma})\Big)dxdt \\
&= \int_\Omega \Big(\overline{S}(x,T) - S^{obs}(x)\Big)z_1(x,T) + \Big(\overline{I}(x,T) - I^{obs}(x)\Big)z_2(x,T)dx \\
&\quad + \Lambda\iint_{Q_T}\nabla(\overline{\beta}, \overline{\gamma})\cdot\nabla\Big((\hat{\beta}, \hat{\gamma}) - (\overline{\beta}, \overline{\gamma})\Big)dxdt, \qquad (64)
\end{aligned}$$

with (z_1, z_2) solution of (60)-(63). From (39)-(42) and (60)-(63), we observe that, we can rewrite the first term of (64) as follows

$$\begin{aligned}
&\int_\Omega \Big(\overline{S}(x,T) - S^{obs}(x)\Big)z_1(x,T) + \Big(\overline{I}(x,T) - I^{obs}(x)\Big)z_2(x,T)dx \\
&\quad = \int_\Omega (p_1 z_1)(x,T) + (p_2 z_2)(x,T)dx = \iint_{Q_T}\frac{\partial}{\partial t}\Big(p_1 z_1 + p_2 z_2\Big)(x,t)dxdt \\
&\quad = \iint_{Q_T}\Big\{d_S p_1 \Delta z_1 + d_I p_2 \Delta z_2 - d_S z_1 \Delta p_1 - d_I z_2 \Delta p_2 \\
&\qquad\qquad + \Big[(\hat{\beta} - \overline{\beta})f(\overline{S}, \overline{I}) - (\hat{\gamma} - \overline{\gamma})\overline{I}\Big](p_2 - p_1)\Big\}dxdt \\
&\quad = \iint_{Q_T}\Big[(\hat{\beta} - \overline{\beta})f(\overline{S}, \overline{I}) - (\hat{\gamma} - \overline{\gamma})\overline{I}\Big](p_2 - p_1)dxdt
\end{aligned}$$

since $\iint_{Q_T}\Big(p_1\Delta z_1 + p_2\Delta z_2 - z_1\Delta p_1 - z_2\Delta p_2\Big)dxdt = 0$. Hence, we conclude the proof of (53). To prove (54)-(55), we apply integration by parts to the last two terms of the integrand in (53).

To prove the elliptic optimality equations (54)–(55), we apply Green's first identity (integration by parts in space) to the regularization terms of (53):

$$\begin{aligned}
&\iint_{Q_T} \Lambda \nabla_x \overline{\beta} \cdot \nabla_x \Big(\hat{\beta} - \overline{\beta}\Big)\, dxdt \\
&\quad = \iint_{Q_T} -\Lambda \Delta_x \overline{\beta} \Big(\hat{\beta} - \overline{\beta}\Big)\, dxdt + \int_{\Gamma} \Lambda (\nabla_x \overline{\beta} \cdot \boldsymbol{\eta}) \Big(\hat{\beta} - \overline{\beta}\Big)\, dSdt, \\
&\iint_{Q_T} \Lambda \nabla_x \overline{\gamma} \cdot \nabla_x \Big(\hat{\gamma} - \overline{\gamma}\Big)\, dxdt \\
&\quad = \iint_{Q_T} -\Lambda \Delta_x \overline{\gamma} \Big(\hat{\gamma} - \overline{\gamma}\Big)\, dxdt + \int_{\Gamma} \Lambda (\nabla_x \overline{\gamma} \cdot \boldsymbol{\eta}) \Big(\hat{\gamma} - \overline{\gamma}\Big)\, dSdt.
\end{aligned}$$

Because the optimizer is assumed to be an interior point, the variational inequality is an equality for arbitrary signed directions. Choosing first directions with compact support in Q_T, the lateral boundary integrals vanish. Factoring out the variations, (53) becomes:

$$\begin{aligned}
\iint_{Q_T} \Big\{ \Big[-\Lambda \Delta_x \overline{\beta} + f(\overline{S}, \overline{I})(p_2 - p_1) \Big] \Big(\hat{\beta} - \overline{\beta}\Big) \\
+ \Big[-\Lambda \Delta_x \overline{\gamma} - \overline{I}(p_2 - p_1) \Big] \Big(\hat{\gamma} - \overline{\gamma}\Big) \Big\}\, dxdt = 0.
\end{aligned}$$

The fundamental lemma of the calculus of variations forces the bracketed terms to vanish in the interior. Allowing signed variations with nonzero traces and using these interior equations then gives the natural homogeneous Neumann conditions on Γ. This establishes (54)–(55). □

3.4. A Uniqueness Result of the Inverse Problem

Theorem 7. *Suppose that the assumptions of Theorem 6 are satisfied, and let $\mathcal{U}_{\mathbf{c}}$ be the subset of $\mathcal{U}_{ad}$ defined as follows:*

$$\mathcal{U}_{\mathbf{c}} = \left\{ (\beta, \gamma) \in \mathcal{U}_{ad} \ : \ \int_{\Omega} (\beta, \gamma)(x, t)\, dx = \mathbf{c} \quad \text{for all } t \in [0, T] \right\}, \tag{65}$$

where $\mathbf{c} \in \mathbb{R}^2_+$ is a fixed positive vector constant. Then, there exists a threshold parameter $\Lambda^* > 0$ such that for any $\Lambda > \Lambda^*$, the solution to the optimization problem (10) is uniquely defined on $\mathcal{U}_{\mathbf{c}}$.

Proof. Let (S, I, p_1, p_2) and $(\hat{S}, \hat{I}, \hat{p}_1, \hat{p}_2)$ be the solutions to the state system (3)–(6) and the adjoint system (39)–(42), associated with the coefficients and observations $(\beta, \gamma, S^{obs}, I^{obs})$ and $(\hat{\beta}, \hat{\gamma}, \hat{S}^{obs}, \hat{I}^{obs})$, respectively. From Theorem 6 and the hypothesis that (β, γ) and $(\hat{\beta}, \hat{\gamma})$ are solutions of (10), we get the following inequalities

$$\iint_{Q_T} \Big\{ \Big[(\overline{\overline{\beta}} - \beta) f(S, I) - (\overline{\overline{\gamma}} - \gamma) I \Big] (p_2 - p_1) \\ + \Lambda \nabla_x \beta \nabla_x \Big(\overline{\overline{\beta}} - \beta \Big) + \Lambda \nabla_x \gamma \nabla_x \Big(\overline{\overline{\gamma}} - \gamma \Big) \Big\} dxdt \geq 0, \quad \forall (\overline{\overline{\beta}}, \overline{\overline{\gamma}}) \in \mathcal{U}_{ad}, \tag{66}$$

$$\iint_{Q_T} \Big\{ \Big[(\underline{\underline{\beta}} - \hat{\beta}) f(\hat{S}, \hat{I}) - (\underline{\underline{\gamma}} - \hat{\gamma}) \hat{I} \Big] (\hat{p}_2 - \hat{p}_1) \\ + \Lambda \nabla_x \hat{\beta} \nabla_x \Big(\underline{\underline{\beta}} - \hat{\beta} \Big) + \Lambda \nabla_x \hat{\gamma} \nabla_x \Big(\underline{\underline{\gamma}} - \hat{\gamma} \Big) \Big\} dxdt \geq 0, \quad \forall (\underline{\underline{\beta}}, \underline{\underline{\gamma}}) \in \mathcal{U}_{ad}. \tag{67}$$

In particular, if we select $(\overline{\overline{\beta}}, \overline{\overline{\gamma}}) = (\hat{\beta}, \hat{\gamma})$ in (66) and $(\underline{\underline{\beta}}, \underline{\underline{\gamma}}) = (\beta, \gamma)$ in (67), by adding the resulting inequalities, we get

$$\Lambda \iint_{Q_T} \Big[|\nabla_x (\hat{\beta} - \beta)|^2 + |\nabla_x (\hat{\gamma} - \gamma)|^2 \Big] dxdt \\ \leq \iint_{Q_T} \Big[(\hat{\beta} - \beta) f(S, I) - (\hat{\gamma} - \gamma) I \Big] (p_2 - p_1) \\ + \Big[(\beta - \hat{\beta}) f(\hat{S}, \hat{I}) - (\gamma - \hat{\gamma}) \hat{I} \Big] (\hat{p}_2 - \hat{p}_1) dxdt. \tag{68}$$

We now analyze and bound the integrand components on the right-hand side of (68). For the transmission components, algebraic rearrangement and the Mean Value Theorem yield:

$$\Big| (\hat{\beta} - \beta) f(S, I)(p_2 - p_1) + (\beta - \hat{\beta}) f(\hat{S}, \hat{I})(\hat{p}_2 - \hat{p}_1) \Big| \\ = \Big| (\hat{\beta} - \beta) \Big[\big(f(S, I) - f(\hat{S}, \hat{I}) \big)(p_2 - p_1) + f(\hat{S}, \hat{I}) \big((p_2 - p_1) - (\hat{p}_2 - \hat{p}_1) \big) \Big] \Big| \\ \leq |\hat{\beta} - \beta| \big(|p_1| + |p_2| \big) \Big(|\partial_1 f(\xi, \chi)| \, |S - \hat{S}| + |\partial_2 f(\xi, \chi)| \, |I - \hat{I}| \Big) \\ + |\hat{\beta} - \beta| \|f\|_{L^\infty(X)} \big(|p_1 - \hat{p}_1| + |p_2 - \hat{p}_2| \big) \\ \leq C |\hat{\beta} - \beta| \Big(|S - \hat{S}| + |I - \hat{I}| + |p_1 - \hat{p}_1| + |p_2 - \hat{p}_2| \Big), \tag{69}$$

where (ξ, χ) is an intermediate point, and the constant C depends on the local Lipschitz constants of f and the uniform bounds derived in Theorem 1 and Theorem 4. Similarly, for the recovery terms, we have:

$$\begin{aligned}
&\Big| - (\hat{\gamma} - \gamma)I(p_2 - p_1) - (\gamma - \hat{\gamma})\hat{I}(\hat{p}_2 - \hat{p}_1)\Big| \\
&\qquad \leq |\hat{\gamma} - \gamma||I|\big(|p_1 - \hat{p}_1| + |p_2 - \hat{p}_2|\big) + |\hat{\gamma} - \gamma|\big(|p_1| + |p_2|\big)|I - \hat{I}|. \quad (70)
\end{aligned}$$

Applying the Young's inequality to (69) and (70), and using the estimates of Theorems 1 and 4, and the stability results on Theorems 2 and 5, we deduce that the estimate (68) implies the inequality

$$\begin{aligned}
&\Lambda \iint_{Q_T} \Big[|\nabla_x(\hat{\beta} - \beta)|^2 + |\nabla_x(\hat{\gamma} - \gamma)|^2\Big] dxdt \\
&\leq C \iint_{Q_T} \Big[|\hat{\beta} - \beta|^2 + |\hat{\gamma} - \gamma|^2 + |\hat{p}_1 - p_1|^2 \\
&\qquad\qquad + |\hat{p}_2 - p_2|^2 + |\hat{S} - S|^2 + |\hat{I} - I|^2\Big] dxdt \\
&\leq C \iint_{Q_T} \Big(|\hat{\beta} - \beta|^2 + |\hat{\gamma} - \gamma|^2\Big) dxdt \\
&\qquad + C \int_{\Omega} \Big(|\hat{S}^{obs} - S^{obs}|^2 + |\hat{I}^{obs} - I^{obs}|^2\Big) dx. \quad (71)
\end{aligned}$$

Since (β, γ) and $(\hat{\beta}, \hat{\gamma})$ belong to the restricted parameter set $\mathcal{U}_{\mathbf{c}}$, their spatial integral discrepancy satisfies $\int_{\Omega}((\hat{\beta}, \hat{\gamma}) - (\beta, \gamma))\,(x,t)dx = 0$ for all $t \in [0, T]$. Consequently, the generalized Poincaré inequality yields the uniform spatial estimate:

$$\begin{aligned}
&\|(\hat{\beta} - \beta)(\cdot, t)\|_{L^2(\Omega)} + \|(\hat{\gamma} - \gamma)(\cdot, t)\|_{L^2(\Omega)} \\
&\qquad \leq C\Big(\|\nabla_x(\hat{\beta} - \beta, \gamma)(\cdot, t)\|_{[L^2(\Omega)]^d} + \|\nabla_x(\hat{\gamma} - \gamma))(\cdot, t)\|_{[L^2(\Omega)]^d}\Big). \quad (72)
\end{aligned}$$

Integrating (72) in time over $[0, T]$ and substituting the result into the first integral on the right-hand side of (71), we can group the gradient terms to find:

$$\begin{aligned}
&(\Lambda - C_0) \iint_{Q_T} \Big(|\nabla_x(\hat{\beta} - \beta)|^2 + |\nabla_x(\hat{\gamma} - \gamma)|^2\Big) dxdt \\
&\qquad\qquad \leq C \int_{\Omega} \Big(|\hat{S}^{obs} - S^{obs}|^2 + |\hat{I}^{obs} - I^{obs}|^2\Big) dx, \quad (73)
\end{aligned}$$

where $C_0 > 0$ is a positive constant incorporating both the regular embedding factors and the Poincaré scaling constant from (72). Then, to establish the conditional uniqueness of the inverse problem solution, we consider the fact that $(\hat{S}^{obs}, \hat{I}^{obs}) = (S^{obs}, I^{obs})$ almost everywhere in Ω. Under this condition, the right-hand side of (73) vanishes identically. By defining the threshold parameter $\Lambda^* = C_0$, it follows that for any regularization choice satisfying $\Lambda > \Lambda^*$, the coefficient matrix factor $(\Lambda - C_0)$ remains strictly positive. Consequently, inequality (73) implies that:

$$\iint_{Q_T} \left(|\nabla_x(\hat{\beta} - \beta)|^2 + |\nabla_x(\hat{\gamma} - \gamma)|^2 \right) dxdt \leq 0, \tag{74}$$

which forces $\nabla_x(\hat{\beta} - \beta) = 0$ and $\nabla_x(\hat{\gamma} - \gamma) = 0$ almost everywhere in Q_T. Then, the identified coefficients can only differ by space-independent functions, i.e., $(\hat{\beta} - \beta)(x,t) = \phi_1(t)$ and $(\hat{\gamma} - \gamma)(x,t) = \phi_2(t)$. Hence, since both parameter pairs are constrained to the restricted admissible subset $\mathcal{U}_{\mathbf{c}}$, integrating their difference over Ω yields:

$$|\Omega|\phi_1(t) = \int_\Omega \big(\hat{\beta}(x,t) - \beta(x,t)\big)dx = c_1 - c_1 = 0, \tag{75}$$

and similarly $|\Omega|\phi_2(t) = 0$ for all $t \in [0,T]$, where $|\Omega| > 0$ denotes the Lebesgue measure of the spatial domain. Thus, $\phi_1(t) = \phi_2(t) = 0$, ensuring that $\hat{\beta} = \beta$ and $\hat{\gamma} = \gamma$ almost everywhere in Q_T. This completes the proof of uniqueness on $\mathcal{U}_{\mathbf{c}}$. $\square$

4. Numerical Solution and Simulations of the Inverse Problem

In this section, we introduce a numerical scheme to approximate the optimization problem (10) and conduct several numerical experiments to illustrate our findings. We assume that the spatio–temporal reaction coefficients β and γ can be parameterized by a finite set of parameters denoted by $\boldsymbol{\theta} = (\theta_1, \ldots, \theta_m) \in \mathbb{R}^m$, such that $\beta(x,t) = \beta(x,t;\boldsymbol{\theta})$ and $\gamma(x,t) = \gamma(x,t;\boldsymbol{\theta})$. Consequently, the continuous constrained optimization problem (10), under this parametric framework, is reduced to the following finite-dimensional parameter identification problem:

$$\left.\begin{array}{l} \overline{\boldsymbol{\theta}} = \min\limits_{\boldsymbol{\theta} \in \Theta_{ad}} \mathcal{J}(\boldsymbol{\theta}), \quad \text{with} \quad \mathcal{J}(\boldsymbol{\theta}) = J(S_{\boldsymbol{\theta}}, I_{\boldsymbol{\theta}}), \\ \text{subject to } (S_{\boldsymbol{\theta}}, I_{\boldsymbol{\theta}}) \text{ being the solution to (3)–(6)} \\ \text{with coefficients } (\beta,\gamma)(x,t) = (\beta,\gamma)(x,t;\boldsymbol{\theta}), \end{array}\right\} \tag{76}$$

where $\Theta_{ad} \subset \mathbb{R}^m$ denotes the set of admissible parameters mapping into $\mathcal{U}_{ad}$. The discretization of the state equations is based mainly on the methodologies described in [37–41]. Concerning the discretization of the inverse problem, we introduce a discrete cost functional which is utilized to solve the resulting parameter estimation problem.

4.1. Discretization of the State System

We assume that the spatial domain Ω where the epidemic event occurs is a hyperrectangle of the form $\Omega = (\underline{L}_1, \overline{L}_1) \times \cdots \times (\underline{L}_d, \overline{L}_d)$, with its boundary denoted by $\partial\Omega$. Let $M_1, \ldots, M_d$, and N be positive integers. We introduce the following grid notations:

$$\begin{aligned}
&\Delta x_i = \frac{\overline{L}_i - \underline{L}_i}{M_i + 1} \quad \text{for } i = 1, \ldots, d, \quad \Delta t = \frac{T}{N}, \\
&\mathcal{K} = \Big\{1, \ldots, M_1\Big\} \times \cdots \times \Big\{1, \ldots, M_d\Big\}, \\
&\overline{\mathcal{K}} = \Big\{0, \ldots, M_1 + 1\Big\} \times \cdots \times \Big\{0, \ldots, M_d + 1\Big\}, \quad \partial\mathcal{K} = \overline{\mathcal{K}} \setminus \mathcal{K}, \\
&\mathbf{k} = (k_1, \ldots, k_d) \in \overline{\mathcal{K}}, \quad x_{\mathbf{k}} = \left(\underline{L}_1 + k_1\Delta x_1,\ \ldots,\ \underline{L}_d + k_d\Delta x_d\right),
\end{aligned}$$

such that the discrete approximations of Ω, $\partial\Omega$, $[0,T]$, Q_T, and Γ are defined by:

$$\begin{aligned}
&\Omega_\Delta = \Big\{x_{\mathbf{k}} \in \Omega \ : \ \mathbf{k} \in \mathcal{K}\Big\}, \quad \partial\Omega_\Delta = \Big\{x_{\mathbf{k}} \in \partial\Omega \ : \ \mathbf{k} \in \partial\mathcal{K}\Big\}, \\
&\mathcal{T}_\Delta = \left\{t_n \in [0,T] \ : \ t_n = n\Delta t \text{ for } n \in \Big\{0, \ldots, N\Big\}\right\}, \\
&Q_\Delta = \Omega_\Delta \times \Big(\mathcal{T}_\Delta \setminus \{t_0\}\Big), \quad \Gamma_\Delta = \partial\Omega_\Delta \times \Big(\mathcal{T}_\Delta \setminus \{t_0\}\Big),
\end{aligned}$$

respectively.

The approximation of a generic function $H : \Omega \times [0,T] \to \mathbb{R}$ at the grid point $(x_{\mathbf{k}}, t_n)$ is denoted by $H_{\mathbf{k}}^n$. The finite difference operators modeling the partial derivatives at $(x_{\mathbf{k}}, t_n)$ are given by the relations:

$$\begin{aligned}
&\frac{\partial w}{\partial t}(x_{\mathbf{k}}, t_n) \approx \frac{w_{\mathbf{k}}^{n+1} - w_{\mathbf{k}}^n}{\Delta t}, \\
&\nabla w(x_{\mathbf{k}}, t_n) \approx \left(\frac{w_{\mathbf{k}+\mathbf{e}_1}^n - w_{\mathbf{k}}^n}{\Delta x_1},\ \ldots,\ \frac{w_{\mathbf{k}+\mathbf{e}_d}^n - w_{\mathbf{k}}^n}{\Delta x_d}\right),
\end{aligned}$$

$$\Delta w(x_{\mathbf{k}}, t_{n+1}) \approx \sum_{i=1}^{d} \frac{w^{n+1}_{\mathbf{k}+\mathbf{e}_i} - 2w^{n+1}_{\mathbf{k}} + w^{n+1}_{\mathbf{k}-\mathbf{e}_i}}{\Delta x_i^2},$$

where $\mathbf{e}_i$ denotes the i-th vector of the canonical basis of $\mathbb{R}^d$. For the non-linear transmission dynamics, we linearize the reaction term $f(S^{n+1}_{\mathbf{k}}, I^{n+1}_{\mathbf{k}})$ around the state at the previous time-step $(S^n_{\mathbf{k}}, I^n_{\mathbf{k}})$. Specifically, we consider the notation $F^{n+1}_{\mathbf{k}}$ and the Taylor expansion:

$$\begin{aligned}
F^{n+1}_{\mathbf{k}} &= F^{n+1}_{\mathbf{k}}(x_{\mathbf{k}}, t_{n+1}, S^{n+1}_{\mathbf{k}}, I^{n+1}_{\mathbf{k}}) \\
&= -\beta(x_{\mathbf{k}}, t_{n+1}) f(S^{n+1}_{\mathbf{k}}, I^{n+1}_{\mathbf{k}}) + \gamma(x_{\mathbf{k}}, t_{n+1}) I^{n+1}_{\mathbf{k}} \\
&= -\beta^{n+1}_{\mathbf{k}} \Big[f(S^n_{\mathbf{k}}, I^n_{\mathbf{k}}) + \partial_1 f(S^n_{\mathbf{k}}, I^n_{\mathbf{k}})(S^{n+1}_{\mathbf{k}} - S^n_{\mathbf{k}}) \\
&\qquad\qquad + \partial_2 f(S^n_{\mathbf{k}}, I^n_{\mathbf{k}})(I^{n+1}_{\mathbf{k}} - I^n_{\mathbf{k}}) \Big] + \gamma^{n+1}_{\mathbf{k}} I^{n+1}_{\mathbf{k}}.
\end{aligned}$$

Consequently, the fully discrete approximation of the initial-boundary value problem (3)–(6) is governed by the following system of algebraic equations:

$$\frac{S^{n+1}_{\mathbf{k}} - S^n_{\mathbf{k}}}{\Delta t} = d_S \sum_{i=1}^{d} \frac{S^{n+1}_{\mathbf{k}+\mathbf{e}_i} - 2S^{n+1}_{\mathbf{k}} + S^{n+1}_{\mathbf{k}-\mathbf{e}_i}}{\Delta x_i^2} + F^{n+1}_{\mathbf{k}}, \qquad \mathbf{k} \in \mathcal{K}, \tag{77}$$

$$\frac{I^{n+1}_{\mathbf{k}} - I^n_{\mathbf{k}}}{\Delta t} = d_I \sum_{i=1}^{d} \frac{I^{n+1}_{\mathbf{k}+\mathbf{e}_i} - 2I^{n+1}_{\mathbf{k}} + I^{n+1}_{\mathbf{k}-\mathbf{e}_i}}{\Delta x_i^2} - F^{n+1}_{\mathbf{k}}, \qquad \mathbf{k} \in \mathcal{K}, \tag{78}$$

$$\nabla S^{n+1}_{\mathbf{k}} \cdot \boldsymbol{\eta}^{n+1}_{\mathbf{k}} = \nabla I^{n+1}_{\mathbf{k}} \cdot \boldsymbol{\eta}^{n+1}_{\mathbf{k}} = 0, \qquad \mathbf{k} \in \partial\mathcal{K}, \tag{79}$$

$$S^0_{\mathbf{k}} = S_0(x_{\mathbf{k}}), \quad I^0_{\mathbf{k}} = I_0(x_{\mathbf{k}}), \qquad \mathbf{k} \in \mathcal{K}. \tag{80}$$

In equation (79), $\boldsymbol{\eta}^{n+1}_{\mathbf{k}}$ is an approximation of the vector $\mathbf{n}$ at $(x_{\mathbf{k}}, t_{n+1})$.

The implementation of (77)-(80) is developed by recursive form on n. More precisely, the scheme begins by discretizing the initial conditions and calculating $\mathbf{u}^0_{\mathbf{k}} = (S^0_{\mathbf{k}}, I^0_{\mathbf{k}})^t$ using the relation (80) and then calculate recursively $\mathbf{u}^{n+1}_{\mathbf{k}} = (S^{n+1}_{\mathbf{k}}, I^{n+1}_{\mathbf{k}})^t$ for $n = 0, \ldots, N-1$ by solving the system defined by (77)–(79). More precisely, let us consider the notation $\mathbf{U}^n$ for the column vector formed by the concatenation of the vectors $\mathbf{u}^n_{\mathbf{k}}$ at each node $\mathbf{k}$ such that $x_{\mathbf{k}} \in \Omega_\Delta \cup \partial\Omega_\Delta$. Then, the scheme (77)–(79), implies that $\mathbf{U}^{n+1}$ can be calculated by solving the linear system

$$\Big[\mathbf{I} - \Delta t\, \mathbb{D} \otimes \mathbf{L} - \Delta t\, \mathbf{J}_{\mathbf{F}}(\mathbf{U}^n)\Big] \mathbf{U}^{n+1} = \mathbf{U}^n + \Delta t\, \mathbf{F}(\mathbf{U}^n) - \Delta t\, \mathbf{J}_{\mathbf{F}}(\mathbf{U}^n)\mathbf{U}^n,$$

where $\mathbf{I}$ is the identity matrix, $\mathbb{D} = \mathrm{diag}(d_S, d_I)$ represents the diagonal diffusion coefficient matrix, $\otimes$ is the matrix Kronecker product, $\mathbf{L}$ is the discrete Laplacian matrix incorporating boundary conditions, $\mathbf{F}$ is a vector constructed as the evaluation of the reaction terms at $\mathbf{U}^n$, and $\mathbf{J_F}$ represents the block-diagonal Jacobian matrix of $\mathbf{F}$. For instance, when $d = 1$ we have that

$$
\begin{aligned}
\mathbf{U}^n &= (S_1^n, \dots, S_M^n, I_1^n, \dots, I_M^n)^t,\\
\mathbf{L} &= \frac{1}{\Delta x^2}\begin{pmatrix}
-1 & 1 & & & \\
1 & -2 & 1 & & \\
 & \ddots & \ddots & \ddots & \\
 & & 1 & -2 & 1\\
 & & & 1 & -1
\end{pmatrix}_{M\times M}\\
\mathbf{F}(\mathbf{U}^n) &= \begin{pmatrix}
-\beta_1^{n+1} f(S_1^n, I_1^n) + \gamma_1^{n+1} I_1^n\\
\vdots\\
-\beta_M^{n+1} f(S_M^n, I_M^n) + \gamma_M^{n+1} I_M^n\\
\beta_1^{n+1} f(S_1^n, I_1^n) - \gamma_1^{n+1} I_1^n\\
\vdots\\
\beta_M^{n+1} f(S_M^n, I_M^n) - \gamma_M^{n+1} I_M^n
\end{pmatrix}.
\end{aligned}
$$

When $d > 1$ the structure of the matrices are similar.

4.2. Discretization of the Optimal Control Problem

For discretization of the inverse problem (10), we begin by considering the discret cost function J_Δ defined as follows

$$
\begin{aligned}
J_\Delta(S_\Delta, I_\Delta) := \frac{\Delta x_1 \dots \Delta x_d}{2} \sum_{\mathbf{k}\in\overline{\mathcal{K}}} \Big[(S_{\mathbf{k}}^N - S_{\mathbf{k}}^{obs})^2 + (I_{\mathbf{k}}^N - I_{\mathbf{k}}^{obs})^2\Big]&\\
+ \frac{\Lambda \Delta x_1 \dots \Delta x_d \Delta t}{2} \sum_{\mathbf{k}\in\overline{\mathcal{K}}} \sum_{n=0}^{N} \Big(|\nabla \beta_{\mathbf{k}}^n|^2 + |\nabla \gamma_{\mathbf{k}}^n|^2\Big),&
\end{aligned}
\tag{81}
$$

where $\nabla \beta_{\mathbf{k}}^n = \nabla_x \beta(x_{\mathbf{k}}, t_n)$ and $\nabla \gamma_{\mathbf{k}}^n = \nabla_x \gamma(x_{\mathbf{k}}, t_n)$. Recalling that (10) is reformulated as the parameter identification problem (76), we consider that the numerical approximation of the inverse problem is given by

$$
\left.
\begin{array}{l}
\overline{\boldsymbol{\theta}} = \min\limits_{\boldsymbol{\theta}\in\Theta_{ad}} \mathscr{J}_\Delta(\boldsymbol{\theta}), \quad \text{with} \quad \mathscr{J}_\Delta(\boldsymbol{\theta}) = J_\Delta(S_\Delta, I_\Delta),\\
\text{subject to } (S_\Delta, I_\Delta) \text{ being the solution of (77)-(80)}\\
\text{with coefficients } (\beta,\gamma)(x_{\mathbf{k}}, t_n) = (\beta,\gamma)(x_{\mathbf{k}}, t_n; \boldsymbol{\theta}).
\end{array}
\right\}
\tag{82}
$$

The finite-dimensional optimization problem (82) can be solved by any optimization algorithm. Specifically, this paper employs a black–box numerical gradient approach via the interior-point method and numerical gradient, implemented using the standard `fmincon` solver in MATLAB.

4.3. Example 1: Identification of β Modeling Non-Pharmaceutical Interventions and γ some Spatial Heterogeneity

In this example we consider that the spatial domain is $\Omega =]0,1[$, the end time of the process is $T = 0.6$, the incidence function is modeled by the mass action function $f(S, I) = SI$, $d_S = d_I = 0.01$, and the initial conditions are given by

$$S_0(x) = 0.99, \quad I_0(x) = 0.01 \exp\left(-(x - 0.5)^2/0.005\right). \tag{83}$$

We note that the initial susceptible population exhibits a uniform spatial distribution of healthy yet vulnerable individuals. Concurrently, the infected population is characterized by a Gaussian profile centered at $x = 0.5$ with a maximum outbreak amplitude of 0.01, where a spatial dispersion parameter of 0.05 determines the geographic concentration or spread of the initial infectious focus.

Furthermore, we assume that the transmission rate β characterizes the temporal evolution of the contagion velocity, thereby incorporating human behavioral changes or non-pharmaceutical interventions. Meanwhile, the recovery rate γ couples spatial heterogeneity, such as healthcare infrastructure, with temporal adaptation, reflecting the medical learning curve. More precisely, these functions are defined as follows:

$$\beta(x, t) = \beta_{\max} - \frac{\alpha_x}{1 + \exp\left(-r_{\text{val}}(t - t^*)\right)}, \quad \text{and} \tag{84}$$

$$\gamma(x, t) = \left(\gamma_{\min} + \frac{\gamma_{\max} - \gamma_{\min}}{1 + \exp\left(-\gamma_{\text{val}}(x - \gamma_0)\right)}\right) + \gamma_{\text{inc}} \left(1 - \exp\left(-\gamma_\eta t\right)\right), \tag{85}$$

where $\beta_{\max}$ is the baseline maximum transmission rate without mitigation measures; α_x is the reduction amplitude from control strategies; t^* is the critical inflection time of policy enforcement; r_{val} is the social implementation rate; $\gamma_{\min}$ and $\gamma_{\max}$ denote the minimum and maximum recovery rates across regions, respectively; γ_0 is the geographical infrastructure threshold; γ_{val} represents the spatial transition gradient; γ_{inc} is the asymptotic temporal increment via medical progress; and γ_η is the systemic learning rate.

We observe that the second term of β models public behavioral changes relative to t^*. Specifically, during the early phase $t \in [0, t^*)$, this negative term remains close to zero, representing the period before containment measures achieve widespread efficacy. Conversely, as time progresses $t \geq t^*$, the term rapidly approaches $-\alpha_x$, capturing the accelerated and cumulative impact of social compliance in lowering transmission. On the other hand, the formulation of γ is explicitly split into two distinct mechanisms: the first and second terms dictate how the recovery rate transitions spatially across the boundary γ_0 due to unequal healthcare access, while the third term captures temporal adaptation, modeling the gradual optimization of clinical treatments and healthcare response.

We assume that $\boldsymbol{\theta} = \Big(\beta_{\text{max}}, \alpha_x, t^*, r_{\text{val}}, \gamma_{\text{min}}, \gamma_{\text{max}}, \gamma_0, \gamma_{\text{val}}, \gamma_{\text{inc}}, \gamma_\eta\Big)$ defines the parameter vector to be identified. The observed profiles are synthetic and are constructed from a numerical simulation of the forward problem using the parameter values $\boldsymbol{\theta}^{\text{obs}}$ listed in Table 1, with spatial and temporal grid sizes of $M = 200$ and $N = 100000$. The simulation using $\boldsymbol{\theta}^{\text{obs}}$ is shown in Figure 1. For the inverse optimization process, the numerical identification is performed on a coarser grid with $M = 100$ and $N = 1000$, initiated from an initial guess $\boldsymbol{\theta}^{\text{ig}}$ to yield the identified parameters $\boldsymbol{\theta}^{\infty}$, and with the Tikhonov regularization parameter $\Lambda = 10^{-5}$. A comparison of the observed, initial guess, and identified profiles is illustrated in Figure 2.

This first test case shows that the optimization framework reliably reconstructs the parametric profiles from the initial guess $\boldsymbol{\theta}^{\text{ig}}$, even under a coarser simulation grid ($M = 100$, $N = 1000$). As the final state profiles in Figure 2a–2b indicate, the identified solutions S^{∞} and I^{∞} align closely with the synthetic observations S^{obs} and I^{obs}, successfully smoothing out the discrepancies introduced by the initial parameters. Figure 2c confirms that the algorithm tracks the transmission rate $\beta(x, t)$ exceptionally well, capturing the exact inflection time $t^* \approx 0.25$ where behavioral mitigation policies take effect. At the same time, the framework accurately calibrates the multi-component recovery rate $\gamma(x, t)$. It successfully captures both the sharp spatial sigmoid transition across the healthcare infrastructure threshold $\gamma_0 = 0.5$ and the asymptotic temporal growth driven by the medical learning rate γ_η. Quantitatively, Table 1 highlights that Tikhonov regularization with $\Lambda = 10^{-5}$ suppresses numerical oscillations. This allows the identified vector $\boldsymbol{\theta}^{\infty}$ to tightly approach the true targets $\boldsymbol{\theta}^{\text{obs}}$, leaving only minor structural deviations in the spatial gradient γ_{val} due to the inherent ill-conditioning of coupled non-linear inverse problems.

Table 1: Numerical values for the observation ($\boldsymbol{\theta}^{\text{obs}}$), the initial guess ($\boldsymbol{\theta}^{\text{ig}}$) and the identified parameters ($\boldsymbol{\theta}^{\infty}$) for example on Subsection 4.3.

	β_{max}	α_x	t^*	r_{val}	γ_{min}
$\boldsymbol{\theta}^{\text{obs}}$	0.5000	0.2000	0.2500	20.0000	0.0500
$\boldsymbol{\theta}^{\text{ig}}$	0.5843	0.1741	0.2912	23.4150	0.0421
$\boldsymbol{\theta}^{\infty}$	0.4947	0.2067	0.2515	23.0890	0.0595
	γ_{max}	γ_0	γ_{val}	γ_{inc}	γ_η
$\boldsymbol{\theta}^{\text{obs}}$	0.1200	0.5000	20.0000	0.0800	0.1000
$\boldsymbol{\theta}^{\text{ig}}$	0.1384	0.4125	17.8920	0.0914	0.0832
$\boldsymbol{\theta}^{\infty}$	0.1005	0.4770	18.0982	0.0805	0.1001

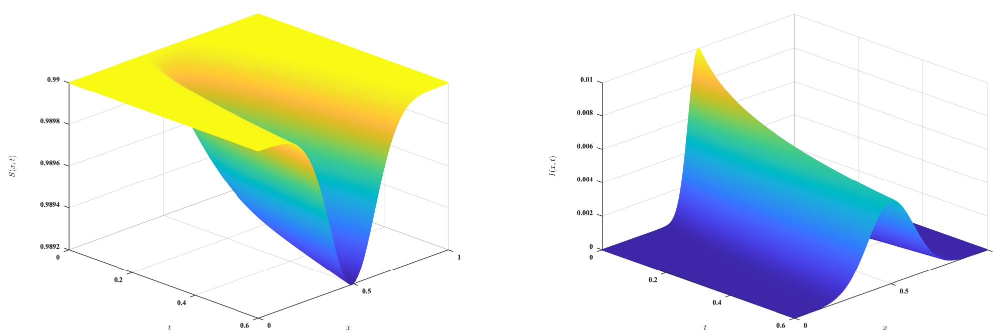

(a) $S(x,t)$ on Q_T.

(b) $I(x,t)$ on Q_T..

Figure 1: Numerical solution for direct problem with the initial data (83) and the numerical values of the parameter given in $\boldsymbol{\theta}^{\text{obs}}$ in Table 1.

4.4. Example 2: Identification for Seasonal Transmission Hotspots (β) and Propagating Vaccination Fronts (γ).

We assume that $Q_T =]0,1[\times(0,1]$, $f(S,I) = SI$, $d_S = d_I = 0.01$, and the initial conditions are given by

$$S_0(x) = \frac{0.2 + \exp(50|x-0.5| - 10)}{1 + \exp(50|x-0.5| - 10)}, \quad I_0(x) = 1.0 - S_0(x). \tag{86}$$

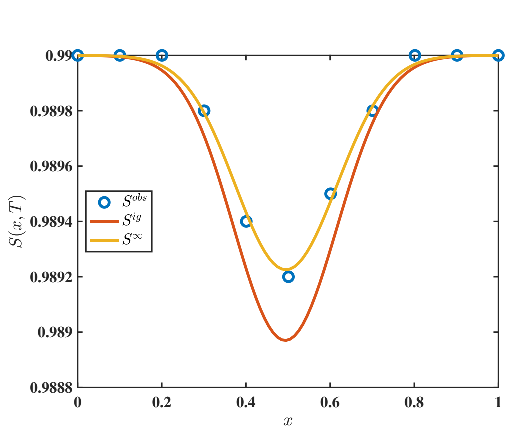

(a) $S(x,T)$.

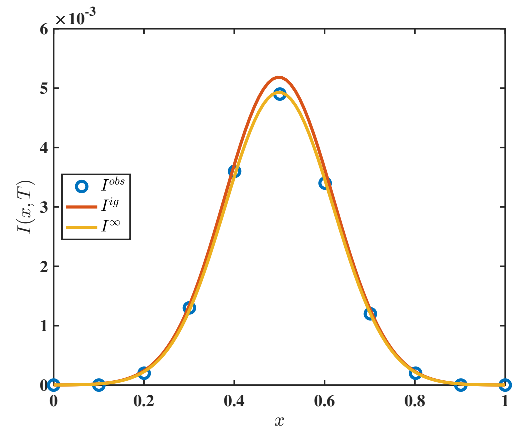

(b) $I(x,T)$.

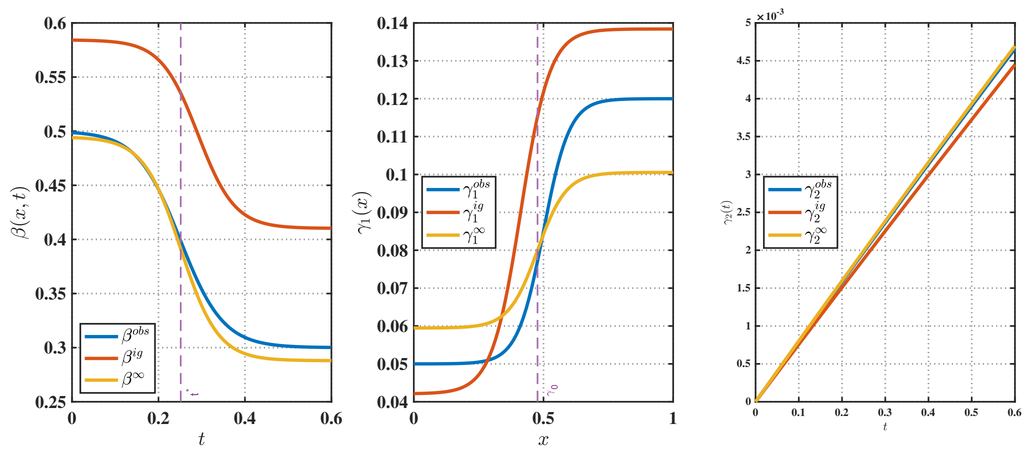

(c) Coefficients β and γ

Figure 2: Comparison of the final profiles for the direct problem solution using the initial data (83) with the reaction coefficients β and γ given in (84)-(85) for the numerical parameter values $\boldsymbol{\theta}^{\text{obs}}$, $\boldsymbol{\theta}^{\text{ig}}$, and $\boldsymbol{\theta}^{\infty}$ provided in Table 1. (a) and (b) Comparison of the final profiles for the susceptible and infected populations, respectively. (c) Comparison of the coefficients: β on the left, $\gamma_1(x) = \gamma_{\min} + \frac{\gamma_{\max}-\gamma_{\min}}{1+\exp(-\gamma_{\text{val}}(x-\gamma_0))}$ in the center, and $\gamma_2(t) = \gamma_{\text{inc}}\left(1 - \exp\left(-\gamma_\eta t\right)\right)$ on the right.

We note that the initial condition for the infected population has a maximum infectious density of 0.8 within the outbreak core, where the geographic center of the infected zone is located at 0.5. Moreover, the radius of the heavily affected area is fixed at 0.2 and the parameter regulating the boundary sharpness is 0.02, modeling a smooth epidemiological transition from the saturated epicenter to the disease-free outskirts. Meanwhile, the initial condition for the susceptible population $S_0(x)$ is complementarily structured, assuming a normalized constant total population density of 1.0. In a broad sense, the consideration of the initial condition in the form of (86) provides a smoothed, step-like distribution for the initial infectious profile, which is motivated by both epidemiological realism and theoretical considerations. From a biological perspective, this formulation accurately depicts an advanced outbreak scenario where the pathogen has thoroughly saturated a localized urban core—establishing a uniform plateau of high infectivity—before spreading toward adjacent, disease-free suburban or rural outskirts. From a theoretical standpoint, avoiding traditional sharp piecewise formulations, such as Heaviside step functions, prevents severe numerical oscillations and gradient indeterminacies during numerical simulations.

On the other hand, for the reaction coefficients, we consider the following parametric forms:

$$\beta(x,t) = \beta_0 \exp\left(-\frac{(x-x_c)^2}{2\sigma^2}\right)\Big(1+\epsilon\sin(\omega t+\phi)\Big), \tag{87}$$

$$\gamma(x,t) = \overline{\gamma}_{\min} + \frac{\overline{\gamma}_{\max}-\overline{\gamma}_{\min}}{1+\exp\left(-\kappa\left(t-\frac{|x-x_0|}{v}\right)\right)}. \tag{88}$$

The transmission rate $\beta(x,t)$ models both geographic localization and environmental periodicity, where the parameter β_0 is a scaling factor establishing the global baseline magnitude of the contact rate, x_c denotes the geographical epicenter where the transmission probability reaches its peak, σ represents the spatial dispersion or physical variance of the outbreak, ϵ represents the relative intensity of the temporal fluctuations, ω defines the angular frequency governing the duration of each epidemiological cycle, and ϕ introduces a phase shift to calibrate the exact timing of the seasonal peaks. Specifically, these effects are governed by a Gaussian distribution that captures the spatial heterogeneity (second factor of β) and a periodic sinusoidal forcing that accounts for cyclical or seasonal variations (third term of β). Meanwhile, the recovery rate $\gamma(x,t)$ models a spatially propagating public health response or medical intervention wave. Here, $\overline{\gamma}_{\min}$ represents the baseline recovery rate prior to intervention, $\overline{\gamma}_{\max}$ denotes the maximum attainable recovery capacity once resources are fully deployed, x_0 identifies the operational headquarters or origin from which medical resources are distributed, and v defines the propagation velocity of this intervention wave across the spatial domain, and κ regulates the activation speed or logistics deployment rate at any given location. Consequently, the dynamic fraction models a smooth sigmoidal transition that captures the delayed arrival and subsequent scaling of healthcare capacity at varying distances from the distribution center.

We assume that $x_c = x_0 = 0.5$ coincident with center of the infected zone in the initial condition (86), the vector of parameters to identify is defined by $\boldsymbol{\theta} = \Big(\beta_0, \sigma, \epsilon, \omega, \phi, \overline{\gamma}_{\min}, \overline{\gamma}_{\max}, \kappa, v\Big)$. The observed profiles are synthetic and are constructed from a numerical simulation of the forward problem using the parameter values $\boldsymbol{\theta}^{\mathrm{obs}}$ listed in Table 2, with spatial and temporal grid sizes of $M = 200$ and $N = 100000$. The simulation using $\boldsymbol{\theta}^{\mathrm{obs}}$ is shown in Figure 3. For the inverse optimization process, the numerical identification is performed on a coarser grid with $M = 100$ and $N = 1000$, the Tikhonov regularization parameter $\Lambda = 10^{-5}$, and its initiated from an initial guess $\boldsymbol{\theta}^{\mathrm{ig}}$ to yield the identified parameters $\boldsymbol{\theta}^{\infty}$. A comparison of the observed, initial guess, and identified profiles is illustrated in Figures 4- 5.

This numerical test evaluates a highly demanding scenario characterized by high infectivity plateaus in the initial states (83) and spatiotemporal oscillations in the governing dynamics. As illustrated in Figures 4a–4b, despite the severe discrepancies present in the initial guess state variables, the optimization algorithm achieves a precise reconstruction of the final-time spatial distributions for both the susceptible and infected populations. Looking at the retrieved coefficients in Figure 4c, the framework demonstrates an outstanding ability to decouple the spatial and temporal components of the transmission rate $\beta(x,t)$. Specifically, the spatial Gaussian variance σ (epicenter focus) and the periodic sinusoidal oscillations $\beta_2(t)$ (seasonal variations) are tracked with high morphological accuracy. Similarly, the propagating recovery front $\gamma(x,t)$ successfully captures the delayed arrival and subsequent logistics deployment rate κ of the medical intervention wave away from the headquarters $x_0 = 0.5$. From a quantitative perspective (Table 2), the identified vector $\boldsymbol{\theta}^{\infty}$ accurately captures the wave propagation velocity ($v^{\infty} = 0.8100$ vs. $v^{\mathrm{obs}} = 0.8000$) and the activation speed κ. However, a slight numerical underestimation is observed in the baseline transmission scaling factor ($\beta_0^{\infty} = 1.6600$ vs. $\beta_0^{\text{obs}} = 2.0000$), which is compensated by structural adjustments in the fluctuation amplitude ϵ and frequency ω. This subtle parameter trade-off highlights the presence of a mild identifiability compromise, typical of complex non-linear inverse problems operating under Tikhonov regularizations ($\Lambda = 10^{-5}$) on coarse discretization grids.

Table 2: Numerical values for the observation ($\boldsymbol{\theta}^{\text{obs}}$), the initial guess ($\boldsymbol{\theta}^{\text{ig}}$) and the identified parameters ($\boldsymbol{\theta}^{\infty}$) for example on Subsection 4.4.

	β_0	σ	ϵ	ω	ϕ
$\boldsymbol{\theta}^{\text{obs}}$	2.000	0.1500	0.3000	6.2832	0.0000
$\boldsymbol{\theta}^{\text{ig}}$	3.500	0.2000	0.2500	5.2000	0.0010
$\boldsymbol{\theta}^{\infty}$	1.6600	0.1702	0.2000	7.0000	0.0100
	$\overline{\gamma}_{\min}$	$\overline{\gamma}_{\max}$	κ	υ	
$\boldsymbol{\theta}^{\text{obs}}$	0.2000	0.8000	20.0000	0.8000	
$\boldsymbol{\theta}^{\text{ig}}$	0.2500	0.9500	25.5500	0.5000	
$\boldsymbol{\theta}^{\infty}$	0.3500	0.7500	19.1500	0.8100	

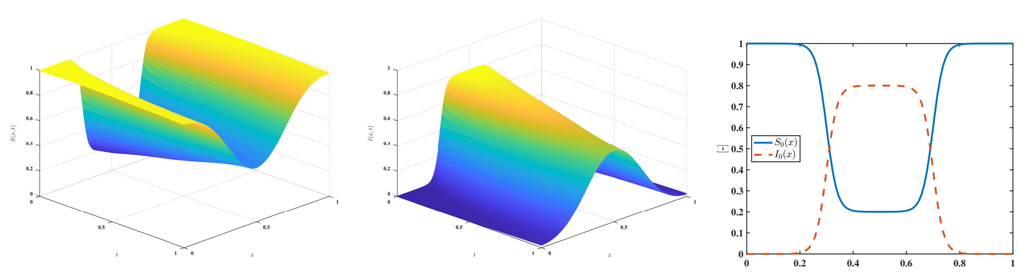

(a) $S(x,t)$. (b) $I(x,t)$. (c) $S_0(x)$ and $I_0(x)$.

Figure 3: Numerical solution for direct problem with the initial data (86) and the numerical values of the parameter given in $\boldsymbol{\theta}^{\text{obs}}$ in Table 2.

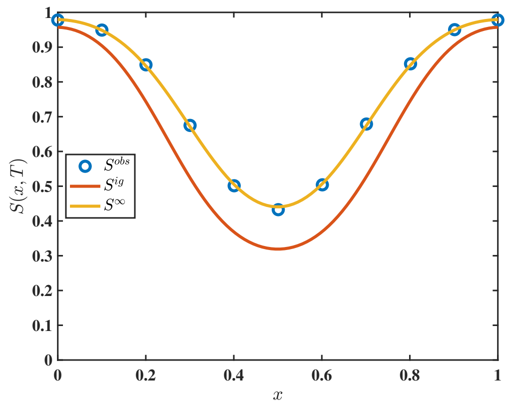

(a) $S(x,T)$.

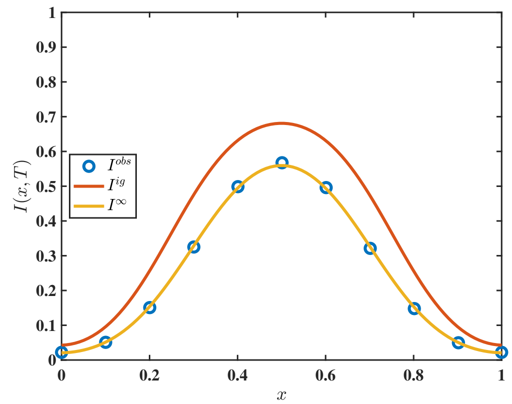

(b) $I(x,T)$.

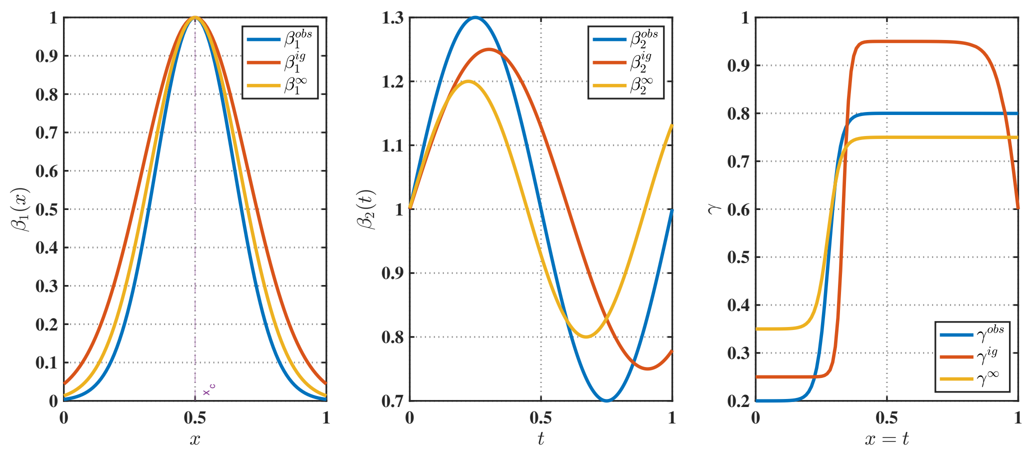

(c) Coefficients β and γ

Figure 4: Comparison of the final profiles for the direct problem solution using the initial data (86) with the reaction coefficients β and γ given in (87)-(88) for the numerical parameter values $\boldsymbol{\theta}^{\text{obs}}$, $\boldsymbol{\theta}^{\text{ig}}$, and $\boldsymbol{\theta}^{\infty}$ provided in Table 2. (a) and (b) Comparison of the final profiles for the susceptible and infected populations, respectively. (c) Comparison of the coefficients: $\beta_1(x) = \exp\left(-\frac{(x-x_c)^2}{2\sigma^2}\right)$ on the left, $\beta_2(t) = \Big(1 + \epsilon \sin(\omega t + \phi)\Big)$ in the center, and $\gamma(x,t)$ along the diagonal $x = t$.

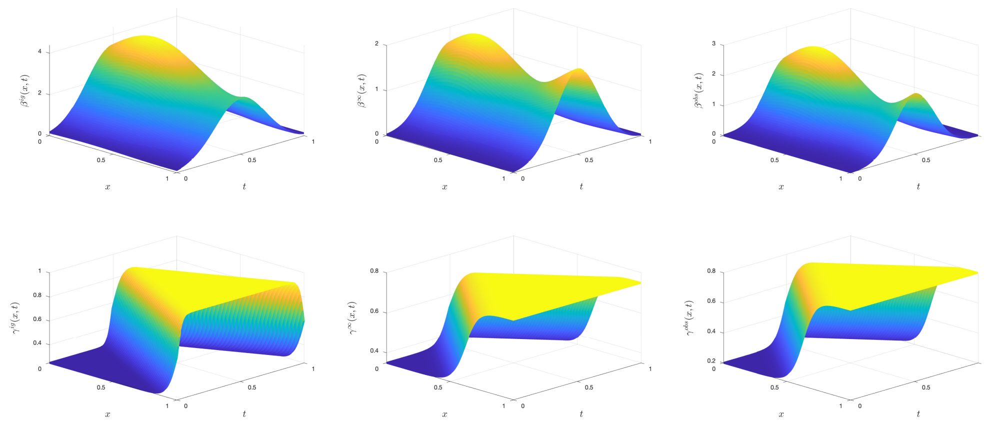

Figure 5: Comparison of the reaction coefficients β and γ given in (87)-(88) for the numerical parameter values $\boldsymbol{\theta}^{\mathrm{obs}}$, $\boldsymbol{\theta}^{\mathrm{ig}}$, and $\boldsymbol{\theta}^{\infty}$ provided in Table 2.

4.5. Example 3: Two Dimensional Spatial Domain with Multiple Outbreaks Foci

In this example, we consider the two-dimensional spatial domain $\Omega =]0,1[\times]0,1[$. Moreover, we assume that $T = 0.6$, $f(S,I) = SI$, $d_S = d_I = 0.01$, and

$$S_0(\mathbf{x}) = 0.99, \tag{89}$$

$$I_0(\mathbf{x}) = 0.01\left[\exp\left(-\frac{\|\mathbf{x}-\mathbf{c}_1\|^2}{0.005}\right) + \exp\left(-\frac{\|\mathbf{x}-\mathbf{c}_2\|^2}{0.005}\right)\right], \tag{90}$$

where $\mathbf{x} = (x_1, x_2)$, $\mathbf{c}_1 = (0.25, 0.25)$ and $\mathbf{c}_2 = (0.75, 0.75)$. Specifically, the initial susceptible population is assumed to be uniformly and spatially homogeneous throughout Ω. Meanwhile, the initial infected population is characterized by two independent active foci localized at $\mathbf{c}_1$ and $\mathbf{c}_2$, each exhibiting a maximum outbreak amplitude of 0.01 and a spatial dispersion controlled by variance of 0.05.

The reaction coefficients are defined as follows:

$$\beta(\mathbf{x},t) = \beta_{\max} - \frac{\alpha_0 + \alpha_1 x + \alpha_2 y}{1 + \exp\left(-r_{\text{val}}(t - t^*)\right)}, \tag{91}$$

$$\begin{aligned}\gamma(\mathbf{x},t) &= \gamma_{\min} + \Big(\gamma_{\max} - \gamma_{\min}\Big) \\ &\quad \times \left[\frac{1}{1 + \exp\left(-\gamma_{\text{val}}\left(\|\mathbf{x}-\mathbf{c}_1\|^2 - R_0\right)\right)} + \frac{1}{1 + \exp\left(-\gamma_{\text{val}}\left(\|\mathbf{x}-\mathbf{c}_2\|^2 - R_0\right)\right)}\right] \\ &\quad + \gamma_{\text{inc}}\left(1 - \exp\left(-\gamma_\eta t\right)\right).\end{aligned} \tag{92}$$

The transmission rate β models a behavioral mitigation that varies linearly across the geographic domain. The recovery rate γ is considered as a bifocal configuration, to ensure mathematical and epidemiological consistency with the initial infection function I_0 in (90), modeling the fact that public health interventions and medical infrastructure are deployed symmetrically at the twin outbreak centers, namely $(0.25, 0.25)$ and $(0.75, 0.75)$. The parameters $\beta_{\max}$, r_{val}, t^*, $\gamma_{\min}$, $\gamma_{\max}$, γ_{val}, γ_{inc}, and γ_η has a same meaning of the one-dimensional version of β and γ given in (84)-(85); α_0, α_1, and α_2 denote the spatial attenuation plane parameters that quantify the intensity of the institutional and behavioral response, where α_0 is the baseline or mean global reduction magnitude, and α_1 and α_2 measure the geographic variations in mitigation efficiency along the x-axis (East-West gradient) and y-axis (North-South gradient), respectively; and R_0 is an operational radius, regulated by the spatial sharpness parameter γ_{val}.

We consider that $\boldsymbol{\theta} = \Big(\beta_{\max}, \alpha_0, \alpha_1, \alpha_2, t^*, r_{\text{val}}, \gamma_{\min}, \gamma_{\max}, \gamma_{\text{val}}, \gamma_{\text{inc}}, \gamma_\eta, R_0\Big)$ is the vector of parameters to identify. The observed profiles are synthetic and are constructed from a numerical simulation of the forward problem using the parameter values $\boldsymbol{\theta}^{\text{obs}}$ listed in Table 3, with spatial and temporal grid sizes of $M = 200$ and $N = 1000$. The simulation using $\boldsymbol{\theta}^{\text{obs}}$ is shown in Figure 6. For the inverse optimization process, the numerical identification is performed on a coarser grid with $M = 100$ and $N = 500$, initiated from an initial guess $\boldsymbol{\theta}^{\text{ig}}$ to yield the identified parameters $\boldsymbol{\theta}^{\infty}$. Additionally, the Tikhonov regularization parameter is set to $\Lambda = 10^{-5}$. A comparison of the observed, initial guess, and identified profiles is illustrated in Figure 7.

This third numerical test evaluates the performance of the identification framework within a two-dimensional spatial setting $\Omega =]0,1[\times]0,1[$ governing dual infection epicenters. As illustrated by the final-time state profiles in Figure 7, the computed optimal fields S^{∞} and I^{∞} accurately replicate the twin-peak morphology of the synthetic observations, successfully eliminating the massive overestimation boundary artifacts present in the initial guess. Regarding the multidimensional coefficient reconstruction, we present the results on Figures 8–10. The Figure 10 show the comparison along the domain diagonal, combined with the spatial contours in Figures 8–9, confirms that the algorithm effectively reconstructs the geometric gradients. Specifically, the planar attenuation parameters $(\alpha_0, \alpha_1, \alpha_2)$ that quantify the East-West and North-South behavioral mitigation gradients are mapped with high spatial fidelity. Simultaneously, the bifocal recovery framework $\gamma(\mathbf{x}, t)$ successfully matches the symmetric logistics capacity deployed around the operating nodes $\mathbf{c}_1$ and $\mathbf{c}_2$. From a quantitative perspective, the parameter values reported in Table 3 reveal an excellent convergence behavior; the identified vector $\boldsymbol{\theta}^{\infty}$ captures the baseline maximum transmission ($\beta_{\max}^{\infty} = 0.4947$ vs. $\beta_{\max}^{\text{obs}} = 0.5000$) and the critical inflection time ($t^{*,\infty} = 0.2515$ vs. $t^{*,\text{obs}} = 0.2500$) with remarkable accuracy. This successful multidimensional calibration, achieved under a coarse optimization grid ($M = 100$, $N = 500$), underscores the structural stability and robust engineering applicability of the proposed discrete optimal control scheme in complex geographic territories.

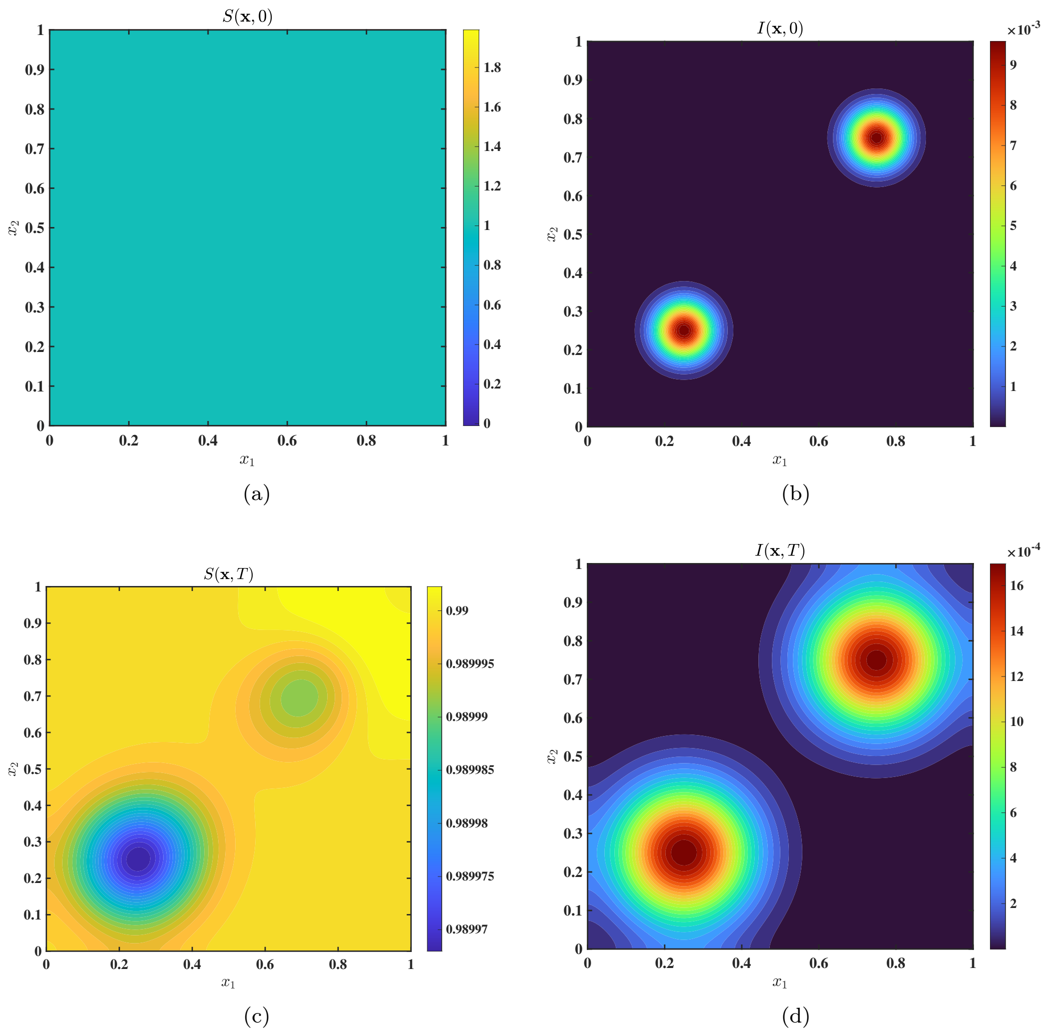

Figure 6: Initial condition and numerical solution for the direct problem: (a)–(b) contours of the initial data (89)–(90), and (c)–(d) contours for the numerical solution calculated with the parameter values given by $\boldsymbol{\theta}^{\text{obs}}$ in Table 3 at the final time T.

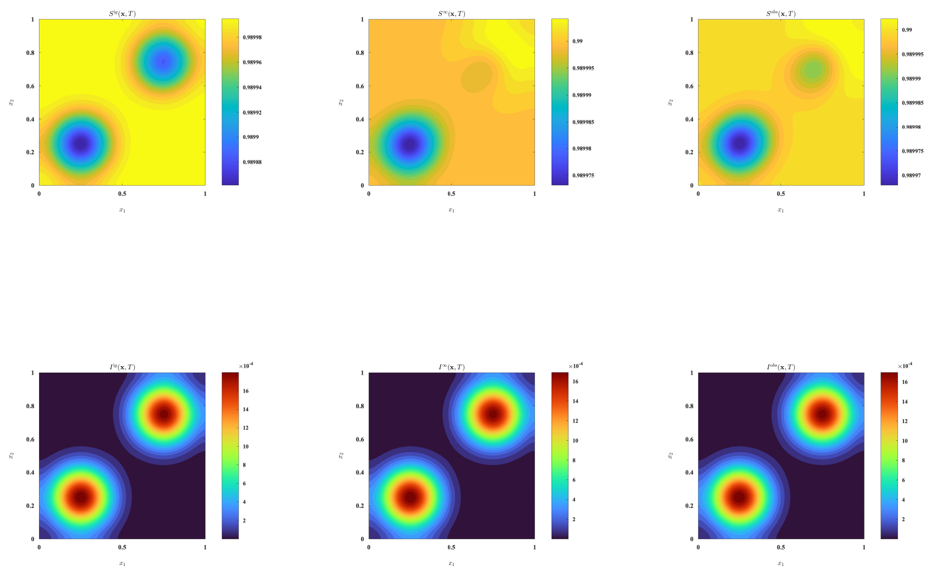

(a) End time profiles.

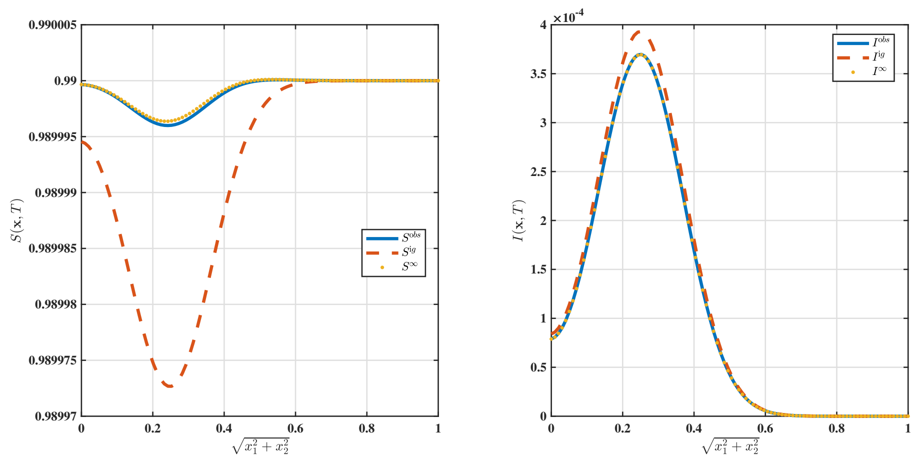

(b) End time profiles through the diagonal

Figure 7: Comparison of state variables and identified coefficients using the initial data (89)–(90) with the spatial forms (91)–(92), evaluated at the parameter vectors $\boldsymbol{\theta}^{\text{obs}}$, $\boldsymbol{\theta}^{\text{ig}}$, and $\boldsymbol{\theta}^{\infty}$ from Table 3: (a) final spatial profiles for the susceptible and infected populations, and (b) behavior of the reaction coefficients β and γ along the diagonal of Ω.

Table 3: Numerical values for the observation ($\boldsymbol{\theta}^{\text{obs}}$), the initial guess ($\boldsymbol{\theta}^{\text{ig}}$) and the identified parameters ($\boldsymbol{\theta}^{\infty}$) for example on Subsection 4.5.

	β_{max}	α_0	α_1	α_2	t^*	r_{val}
$\boldsymbol{\theta}^{\text{obs}}$	0.6000	0.1500	0.0500	0.05000	0.3500	15.000
$\boldsymbol{\theta}^{\text{ig}}$	0.7000	0.1000	0.0700	0.0700	0.4000	18.0000
$\boldsymbol{\theta}^{\infty}$	0.5758	0.1460	0.0625	0.0625	0.3471	17.9139
	γ_{min}	γ_{max}	γ_{val}	γ_{inc}	γ_{η}	R_0
$\boldsymbol{\theta}^{\text{obs}}$	0.1000	0.3500	10.0000	0.1200	2.0000	0.0800
$\boldsymbol{\theta}^{\text{ig}}$	0.2000	0.4000	12.0000	0.1400	2.5000	0.0900
$\boldsymbol{\theta}^{\infty}$	0.1527	0.3540	11.9239	0.1300	2.0933	0.0747

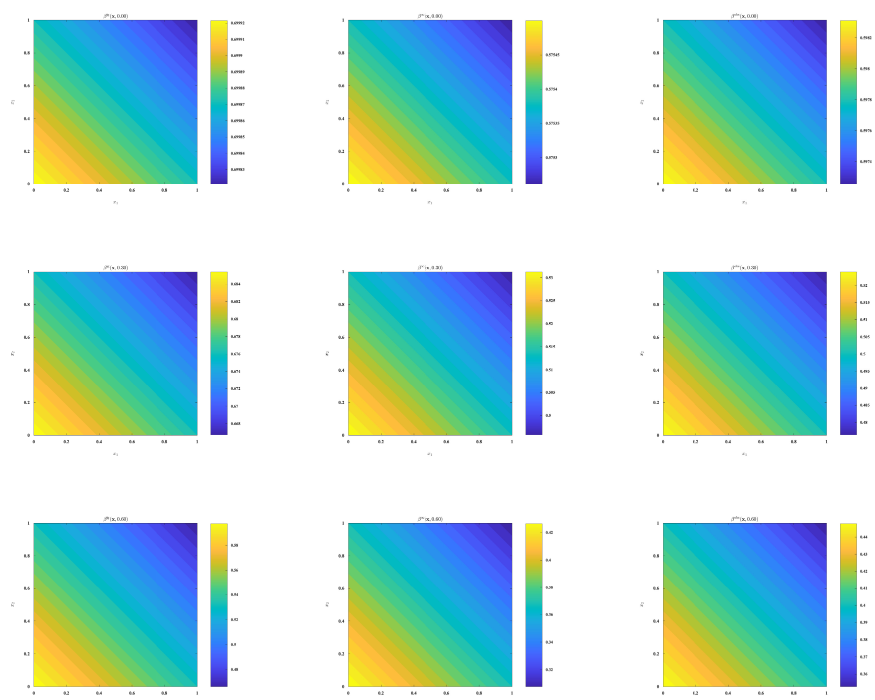

Figure 8: Comparison of the spatial contours for β evaluated at the parameter vectors $\boldsymbol{\theta}^{\text{obs}}$, $\boldsymbol{\theta}^{\text{ig}}$, and $\boldsymbol{\theta}^{\infty}$ from Table 3, displayed across three distinct time steps.

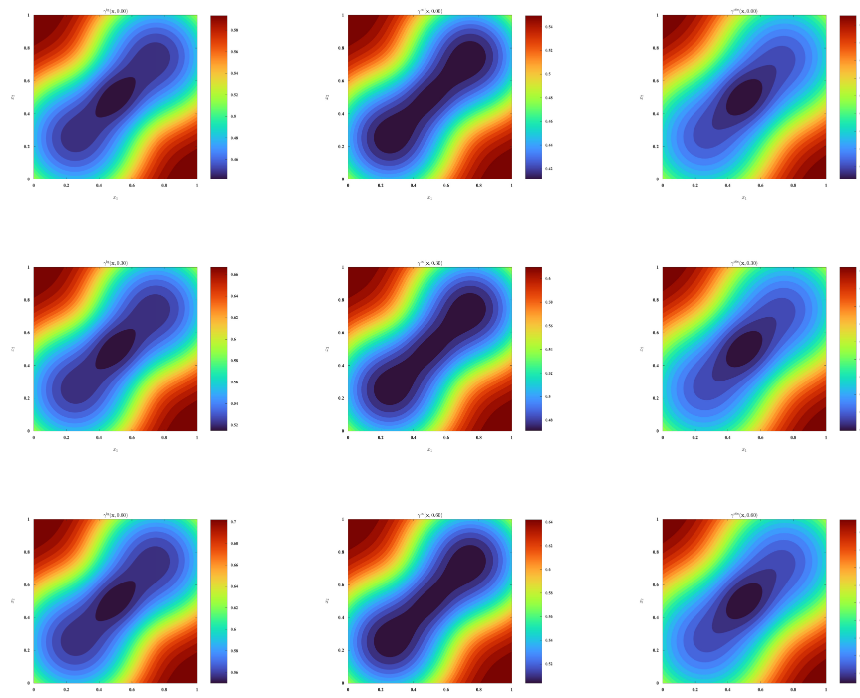

Figure 9: Comparison of the spatial contours for γ evaluated at the parameter vectors $\boldsymbol{\theta}^{\mathrm{obs}}$, $\boldsymbol{\theta}^{\mathrm{ig}}$, and $\boldsymbol{\theta}^{\infty}$ from Table 3, displayed across three distinct time steps.

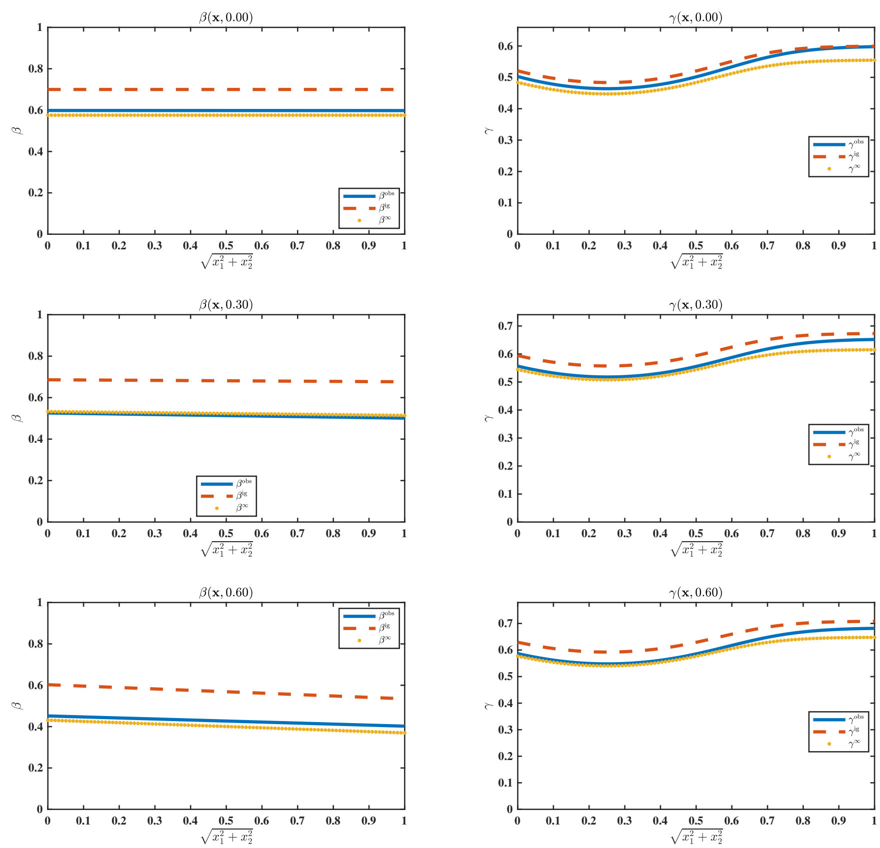

Figure 10: Behavior of the reaction coefficients β and γ along the diagonal of Ω, evaluated at the parameter vectors $\boldsymbol{\theta}^{\mathrm{obs}}$, $\boldsymbol{\theta}^{\mathrm{ig}}$, and $\boldsymbol{\theta}^{\infty}$ from Table 3, displayed across three distinct time steps.

5. Conclusion

In this work, we have studied a mathematical framework for the inverse problem of identifying spatio-temporal reaction coefficients (β, γ) in a generalized SIS reaction–diffusion system. The analysis addresses the state and adjoint systems, existence of an optimal control, first-order necessary optimality conditions, stability estimates, and conditional uniqueness on a fixed-mean admissible subset. The numerical section illustrates a finite-dimensional parameter-identification procedure in one and two spatial dimensions. The reported examples attain small final-time tracking errors for the chosen synthetic data and a regularization parameter $\Lambda = 10^{-5}$.

A critical limitation observed in the parameter identification is the sensitivity of the optimization trajectory to the initial guess $\boldsymbol{\theta}^{\mathrm{ig}}$, where certain tightly coupled parameters require high-quality final-time spatial data to avoid localized structural stagnation. Future research directions will address the extension of this optimization framework to identify unknown functions in reaction terms and diffusion coefficients and validate the algorithms using real-world clinical datasets from specific historical epidemics.

Acknowledgments

This research was funded by National Agency for Research and Development, ANID-Chile, through FONDECYT projects 1230560, VRID UdeC project 2026001602INV, and ANID-Chile through Centro de Modelamiento Matemático (FB210005); the Project supported by the Competition for Research Regular Projects, year 2023, code LPR23-03, Universidad Tecnológica Metropolitana; and Universidad del Bío-Bío through the Regular Research Project RE2547710 and FAPEI FP2631905.

References

[1] R. Anderson, R.M. May, Infectious Diseases of Humans: Dynamics and Control, Oxford University Press, Oxford, 1991.

[2] N. Bacaër, A Short History of Mathematical Population Dynamics, Springer, London, 2011. DOI: 10.1007/978-0-85729-115-8

[3] R. Cherniha, V. Davydovych, Nonlinear Reaction-Diffusion Systems: Conditional Symmetry, Exact Solutions and Their Applications in Biology, Vol. 2196, Springer, Cham, 2017. DOI: 10.1007/978-3-319-65467-6

[4] M. Martcheva, An Introduction to Mathematical Epidemiology, Vol. 61, Springer, New York, 2015. DOI: 10.1007/978-1-4899-7612-3

[5] F. Brauer, P. Driessche, J. Wu, Mathematical Epidemiology, Vol. 1945, Springer, Berlin, 2008. DOI: 10.1007/978-3-540-78911-6

[6] E. Kuhl, Computational Epidemiology: Data-Driven Modeling of COVID-19, Springer, Cham, 2021. DOI: 10.1007/978-3-030-82890-5

[7] F. Brauer, C. Castillo-Chavez, Z. Feng, Mathematical Models in Epidemiology, Vol. 32, Springer, New York, 2019. DOI: 10.1007/978-1-4939-9828-9

[8] W.O. Kermack, A.G. McKendrick, A contribution to the mathematical theory of epidemics, Proc. R. Soc. Lond. Ser. A 115 (1927) 700–721. DOI: 10.1098/rspa.1927.0118

[9] F. Brauer, Models for the spread of universal fatal diseases, J. Math. Biol. 28 (1990) 451–462. DOI: 10.1007/BF00178328

[10] H. Behncke, Optimal control of deterministic epidemics, Optim. Control Appl. Methods 21 (2000) 269–285. DOI: 10.1002/oca.678

[11] H.W. Hethcote, P. van den Driessche, Some epidemiological models with nonlinear incidence, J. Math. Biol. 29 (2000) 271–287. DOI: 10.1007/BF00160539

[12] H. McCallum, N. Barlow, J. Hone, How should pathogen transmission be modelled?, Trends Ecol. Evol. 16 (2001) 295–300. DOI: 10.1016/s0169-5347(01)02144-9

[13] X.-Z. Zhang, X.-N. Liu, Backward bifurcation of an epidemic model with saturated treatment function, J. Math. Anal. Appl. 348 (1) (2008) 433–443. DOI: 10.1016/j.jmaa.2008.07.042

[14] Y. Tao, M. Winkler, Analysis of a chemotaxis-SIS epidemic model with unbounded infection force, Nonlinear Anal. Real World Appl. 71 (2023) 103820. DOI: 10.1016/j.nonrwa.2022.103820

[15] Z. Jiao, I. Jadlovska, T. Li, Analysis of an SIS reaction-diffusion-chemotaxis limitation and standard incidence, Discrete Contin. Dyn. Syst. Ser. B 29 (9) (2024) 3731–3743. DOI: 10.3934/dcdsb.2024021

[16] M. Yan, Global smooth solutions of the chemotaxis-SIS epidemic model with nonlinear incidence rate, Z. Angew. Math. Phys. 76 (3) (2025) 95. DOI: 10.1007/s00033-025-02476-z

[17] Q. Zhang, On small-data solution of the chemotaxis-SIS epidemic system with bilinear incidence rate, Nonlinear Anal. Real World Appl. 77 (2024) 104063. DOI: 10.1016/j.nonrwa.2024.104063

[18] A.P. Farrell, J.P. Collins, A.L. Greer, H.R. Thieme, Do fatal infectious diseases eradicate host species?, J. Math. Biol. 77 (6-7) (2018) 2103–2164. DOI: 10.1007/s00285-018-1249-3

[19] N.V. Krylov, Lectures on Elliptic and Parabolic Equations in Sobolev Spaces, American Mathematical Society, Providence, 2008. DOI: 10.1090/gsm/096

[20] O.A. Ladyzhenskaya, V. Solonnikov, N. Ural'ceva, Linear and Quasi-linear Equations of Parabolic Type, American Mathematical Society, Providence, 1968. DOI: 10.1090/mmono/023

[21] G.M. Lieberman, Second Order Parabolic Differential Equations, World Scientific, River Edge, 1996. DOI: 10.1142/3302

[22] L.C. Evans, Partial Differential Equations, second ed., Graduate Studies in Mathematics, vol. 19, American Mathematical Society, Providence, RI, 2022. DOI: 10.1090/gsm/019

[23] M.D. Gunzburger, Perspectives in Flow Control and Optimization, SIAM, Philadelphia, 2003. DOI: 10.1115/1.1623758

[24] N.C. Apreutesei, An optimal control problem for a pest, predator, and plant system, Nonlinear Anal. Real World Appl. 13 (2012) 1391–1400. DOI: 10.1016/j.nonrwa.2011.11.004

[25] Q. Chen, J.J. Liu, Solving an inverse parabolic problem by optimization from final measurement data, J. Comput. Appl. Math. 193 (2006) 183–203. DOI: 10.1016/j.cam.2005.06.003

[26] A. Coronel, L. Friz, I. Hess, M. Zegarra, On the existence and uniqueness of an inverse problem in epidemiology, Appl. Anal. 100 (3) (2021) 513–526. DOI: 10.1080/00036811.2019.1608964

[27] A. Coronel, F. Huancas, M. Sepúlveda, A note on the existence and stability of an inverse problem for a SIS model, Comput. Math. Appl. 77 (12) (2019) 3186–3194. DOI: 10.1016/j.camwa.2019.01.031

[28] A. Coronel, F. Huancas, M. Sepúlveda, Identification of space distributed coefficients in an indirectly transmitted diseases model, Inverse Probl. 35 (11) (2019) 115001. DOI: 10.1088/1361-6420/ab3a86

[29] M. Cristofol, P. Gaitan, K. Niinimäki, O. Poisson, Inverse problem for a coupled parabolic system with discontinuous conductivities: one-dimensional case, Inverse Probl. Imaging 7 (1) (2013) 159–182. DOI: 10.3934/ipi.2013.7.159

[30] M. Cristofol, P. Gaitan, H. Ramoul, M. Yamamoto, Identification of two coefficients with data of one component for a nonlinear parabolic system, Appl. Anal. 91 (11) (2012) 2073–2081. DOI: 10.1080/00036811.2011.583240

[31] M. Cristofol, L. Roques, The inverse problem of determining several coefficients in a nonlinear Lotka-Volterra system, Inverse Probl. 28 (7) (2012) 075007. DOI: 10.1016/j.crma.2012.04.019

[32] M. Cristofol, L. Roques, An inverse problem involving two coefficients in a nonlinear reaction-diffusion equation, C. R. Math. Acad. Sci. Paris 350 (9-10) (2012) 469–473. DOI: 10.1016/j.crma.2012.04.019

[33] B. Wu, J. Yu, Hölder stability of an inverse problem for a strongly coupled reaction-diffusion system, IMA J. Appl. Math. 82 (2) (2017) 424–444. DOI: 10.1093/imamat/hxw058

[34] H. Xiang, B. Liu, Solving the inverse problem of an SIS epidemic reaction–diffusion model by optimal control methods, Comput. Math. Appl. 70 (2015) 805–819. DOI: 10.1016/j.camwa.2015.05.025

[35] A. Coronel, F. Huancas, M. Sepúlveda, Identification of a power-like reaction term in a reaction-diffusion SIS model, Preprint 2026-10, CI2MA, Universidad de Concepción, Chile, 2026.

[36] Du, Z., Peng, R. A priori estimates for solutions of a class of reaction-diffusion systems. J. Math. Biol. 72, 1429–1439 (2016). DOI: 10.1007/s00285-015-0914-z

[37] D. Hoff, Stability and convergence of finite difference methods for systems of nonlinear reaction-diffusion equations, SIAM J. Numer. Anal. 15 (1978) 1161–1177. DOI: 10.1137/0715077

[38] X. Liu, Z.W. Yang, Numerical analysis of a reaction-diffusion susceptible-infected-susceptible epidemic model, Comput. Math. Appl. 41 (2022) 392. DOI: 10.1007/s40314-022-02113-9

[39] X. Liu, Z.W. Yang, Y.M. Zeng, Global numerical analysis of an improved IMEX numerical scheme for a reaction diffusion SIS model in advective heterogeneous environments, Comput. Math. Appl. 144 (2023) 264–273. DOI: 10.1016/j.camwa.2023.06.018

[40] L. Lopez, Stability and asymptotic behaviour for the numerical solution of a reaction-diffusion model for a deterministic diffusive epidemic, IMA J. Numer. Anal. 3 (3) (1983) 341–351. DOI: 10.1093/imanum/3.3.341

[41] S. Yang, X. Liu, Numerical threshold stability analysis of a positivity-preserving IMEX numerical scheme for a nonlinear age-space structured SIR epidemic model, Comput. Appl. Math. 43 (2024) 240. DOI: 10.1007/s40314-024-02768-6

Centro de Investigación en Ingeniería Matemática (CI^{2}MA)

PRE-PUBLICACIONES 2026

2026-18 Gonzalo A. Benavides, Sergio Caucao, Gabriel N. Gatica, Yuri D. Sobral: *New Banach spaces-based mixed finite element methods for steady-state flows of magnetic fluids*

2026-19 Fahim Aslam, Marcelo Cavalcanti, Zayd Hajjej, You Haiyang Lin Bo, Mauricio Sepúlveda: *Blow-up of a Lamé system with fractional damping and infinite memory: theoretical and numerical study*

2026-20 Gabriel N. Gatica, Salim Meddahi: *A hybridizable discontinuous Galerkin method for the elasto–acoustic transmission problem*

2026-21 Idulfo Arrocha, Raimund Bürger, María Gómez, Yolanda Vásquez: *Modeling and numerical simulation of the colonization of plant growth-promoting bacteria in the rice rhizosphere*

2026-22 Abraham J. Arenas, Juan Barajas-Calonge, Gilberto González-Parra, Luis M. Villada: *Convergence analysis of a nonstandard finite volume method for a diffusion-production-destruction model*

2026-23 Juan Barajas-Calonge, Raimund Bürger, Stefan Diehl, Luis M. Villada: *A network of conservation laws with discontinuous fluxes and source terms modeling countercurrent decantation*

2026-24 Raimund Bürger, Bakhtiyor Khuzhayorov, Usmonali Saydullaev, Iroda Beknazarova: *Numerical simulation of filtration of a suspension through a radial filter with given flow rate*

2026-25 Fernando Muñoz García, Fernando Roldán: *Forward-reflected-backward algorithm with linesearch*

2026-26 Eider Aldana, Ricardo Oyarzúa: *A Lagrange multiplier approach for fluid-flow problem with inhomogeneous mixed boundary conditions*

2026-27 Jean-Christophe Pesquet, Fernando Roldán: *Nonlinear forward-backward algorithm for solving non-monotone+Lipschitz inclusions with applications to adjoint mismatch problems*

2026-28 Juan Barajas-Calonge, Julio Careaga, Luis M. Villada: *Invariant-region-preserving high-order schemes for a model of reactive sedimentation*

2026-29 Aníbal Coronel, Fernando Huancas, Mauricio Sepúlveda: *Theoretical analysis and numerical validation of an inverse problem in a SIS reaction–diffusion system, Part 1: Identification of transmission and recovery rates*

Para obtener copias de las Pre-Publicaciones, escribir o llamar a: Director, Centro de Investigación en Ingeniería Matemática, Universidad de Concepción, Casilla 160-C, Concepción, Chile, Tel.: 41-2661324, o bien, visitar la página web del centro: http://www.ci2ma.udec.cl

Centro de Investigación en
Ingeniería Matemática (CI^{2}MA)
Universidad de Concepción

Casilla 160-C, Concepción, Chile
Tel.: 56-41-2661324/2661554/2661316
http://www.ci2ma.udec.cl